

**FRICTION STIR WELDING: THERMAL EFFECTS OF A PARAMETRIC STUDY ON
BUTT AND LAP WELDS**

A Thesis by

Rajesh Naidu

Bachelor of Engineering, Shivaji University, India, 2003

Submitted to the Department of Mechanical Engineering
and the faculty of Graduate School of
Wichita State University
in partial fulfillment of
the requirements for the degree of
Master of Science

December 2006

FRICTION STIR WELDING: THERMAL EFFECTS OF A PARAMETRIC STUDY ON BUTT AND LAP WELDS

I have examined the final copy of this thesis for form and content and recommend that it to be accepted in partial fulfillment of the requirements for the degree of Master of Science, with a major in Mechanical Engineering.

Kurt A.Soschinske, Committee Chair

We have read this thesis and recommend its acceptance:

Jorge E.Talia, Committee Member

Mehmet Bayram Yildirim, Committee Member

ACKNOWLEDGEMENT

I would like to express my gratitude to my academic advisor, Dr. Kurt A. Soschinske for his outstanding and constant support, patience and guidance during my entire graduate studies. Working with him was a truly memorable experience. I would also like to express my sincere appreciation to my distinguished committee members, Dr. Jorge E. Talia and Dr. Mehmet Bayram Yildirim for their valuable assistance, time and help in reviewing this manuscript.

My sincere appreciation to Dr. Mir Z.Khandkar from the University of South Carolina and Dr. Christian Widener from the National Institute for Aviation Research (NIAR) for their valuable suggestions and time during this research.

I am extremely grateful to my parents and sisters for their love, support, and constant encouragement throughout my academic years. Special thanks to Livermore Software Technology Corporation (LSTC) for providing me with important conference proceedings and software documentation.

ABSTRACT

The purpose of this thesis was to develop and validate finite element models of the friction stir welding process for butt and lap welds for specific experimental cases that in effect enhances the predictability of temperature evolution in the joined workpiece. Significant research has been conducted on butt weld thermal process but limited study has been conducted on lap welds. Through examination of several process parameters critical to both weld and lap weld operations insights into process characterization of process parameters could be made. In this study three dimensional finite element heat transfer models using the commercial code LS-DYNA were developed to obtain the temperature distribution in the workpiece for two types of welds, namely butt joints and lap joints. For the lap weld model a step function for thermal conductance between sheets was applied to account for varying contact resistance. The developed finite element models were validated with published experimental data. Parametric studies were performed involving both types of welds including process parameters such as tool travel rate and rotational tool velocity for different aluminium alloys.

TABLE OF CONTENTS

Chapter	Page
1. INTRODUCTION.....	1
1.1 Background	1
1.2 Types of FSW	2
1.3 Advantages and Disadvantages.....	4
1.4 Applications	5
1.5 Problem Statement	5
1.6 Study Objectives	6
1.7 Methodology	6
2. LITERATURE REVIEW.....	8
2.1 Thermal Process Models of FSW of Butt and Lap Welds	8
2.2 FSW Process Parameters.....	14
3. METHODOLOGY	16
3.1 Introduction to MSC.Patran 2005	16
3.2 Introduction to LS-DYNA	17
3.2.1 LS-DYNA File Structure	18
3.2.2 LS-DYNA Thermal Weld Model.....	18
3.3 Introduction to LS-PREPOST.....	19
3.4 Model Development for FSW of a Butt Weld	20
3.4.1 Geometry.....	20
3.4.2 Mesh Development	21
3.4.3 Material Properties	21
3.4.4 Boundary Conditions	23
3.4.5 Heat Input Implementation	25
3.5 Model Development for FSW of a Lap Weld.....	27
3.5.1 Geometry.....	27
3.5.2 Mesh Development	28
3.5.3 Material Properties	28
3.5.4 Boundary Conditions	29
3.5.5 Heat Input Implementation	32
3.6 Parametric Study Definitions for Butt and Lap Welds	33
3.6.1 Butt Weld Model Correlation and Parametric Study Definitions	33
3.6.2 Lap Weld Model Correlation and Parametric Study Definitions.....	37
4. RESULTS AND DISCUSSIONS	43
4.1 Butt Weld Simulations	43
4.2 Lap Weld Simulations.....	55

5.	CONCLUSIONS AND RECOMMENDATIONS	67
5.1	Conclusions.....	67
5.2	Recommendations.....	69
	REFERENCES.....	70
	APPENDIX	73

LIST OF TABLES

Table	Page
3.1 Thermal Material Properties of Al6061-T6 Alloy	22
3.2 Thermal Material Properties of Al5052-H32 Alloy	22
3.3 Thermal Material Properties of Al7050-T7451 Alloy	22
3.4 Thermal Material Properties of Al2024-T3 Alloy	29
3.5 Model Descriptions for Various Butt Weld Cases in the Parametric Study	36
3.6 Correlation Models for a FSW of Lap Weld.....	38
3.7 Model Descriptions for Various Lap Weld Cases in the Parametric Study	41
3.8 Model Description for Case 4 of Lap Weld in the Parametric Study	42
4.1 Summary of Peak Temperatures for Butt Weld of Al6061-T6.....	54
4.2 Summary of Peak Temperatures for Butt Weld of Al5052-H32	54
4.3 Summary of Peak Temperatures for Butt Weld of Al7050-T7451	54
4.4 Summary of Results for Case 4 of Lap Weld	65
4.5 Summary of Peak Temperatures Obtained for Case 1 of Lap Weld.....	66
4.6 Summary of Peak Temperatures Obtained for Case 2 of Lap Weld.....	66
4.7 Summary of Peak Temperatures Obtained for Case 3 of Lap Weld.....	66

LIST OF FIGURES

Figure	Page
1.1 Schematic Representation of FSW of a Butt Joint.....	3
1.2 Schematic of an Overlap FSW Configuration.....	3
1.3 Schematic of a Friction Stir Spot Welding Process	4
2.1 Schematic Representation of Boundary Conditions.....	10
3.2 J. Goldak's Heat Source Model.....	19
3.4 Geometric Model of Two Plates to be Butt Welded	20
3.5 Finite Element Model of the Sheets	21
3.6 Comparison of Thermal Properties for Different Aluminium alloys.....	23
3.7 Schematic Representation of Boundary Conditions for FSW of Butt Weld.....	25
3.8 MSC.Patran Model of Two Sheets being Lap Welded	27
3.9 Finite Element Model of the Two Sheets Lapped Together	28
3.10 Schematic Representation of Boundary Conditions for FSW of Lap Weld	31
3.11 Comparison of Simulated and Experimental Results Recorded Perpendicular to Weld-line on Top Surface for Al6061T6 at a Distance of 190 mm from Edge of Sheet.....	34
3.12 Comparison of Simulated and Experimental Results Recorded Perpendicular to Weld-line on Mid Surface for Al6061T6 at a Distance of 190 mm from Edge of Sheet	35
3.13 Comparison of Simulated and Experimental Results Recorded Perpendicular to Weld-line on Bottom Surface for Al6061T6 at a Distance of 190 mm from Edge of Sheet	35
3.14 Correlation of Case 2 and Case 3 of Lap Weld with Best Fit (0% error) Line	39
3.15 Comparison of Simulated and Experimental Results Recorded Perpendicular to Weld-line on Top Surface for Al5454-O at a Distance of 190 mm from Edge of Sheet.....	40
3.16 Comparison of Simulated and Experimental Results Recorded Perpendicular to Weld-line on Mid Surface for Al5454-O at a Distance of 190 mm from Edge of Sheet.....	40
4.1.1 Top Surface Temperature Contours after 2 Sec at Tool Travel Rate of 90 mm/min.....	43

4.1.2	Top Surface Temperature Contours after 60 Sec at Tool Travel Rate of 90 mm/min.....	44
4.1.3	Top Surface Temperature Contours After 107 Sec at Tool Travel Rate of 90 mm/min...	44
4.1.4	Temperature Contours Through the Weld Seam at a Tool Travel Rate of 90 mm/min....	45
4.1.5	Instantaneous Temperature Profiles Perpendicular to Weld Line at 90 mm/min	45
4.1.6	Instantaneous Temperature Profiles Perpendicular to Weld Line at 115 mm/min	46
4.1.7	Instantaneous Temperature Profiles Perpendicular to Weld Line at 140 mm/min	46
4.1.8	Variation of Temperature on Top Surface for Different Tool Travel Rates	47
4.2.1	Instantaneous Temperature Profiles Perpendicular to Weld Line at 115 mm/min	48
4.2.2	Instantaneous Temperature Profiles Perpendicular to Weld Line at 140 mm/min	49
4.2.3	Instantaneous Temperature Profiles Perpendicular to Weld Line at 175 mm/min	49
4.2.4	Variation of Temperature on Top Surface for Different Tool Travel Rates	50
4.3.1	Instantaneous Temperature Profiles Perpendicular to Weld Line at 140 mm/min	51
4.3.2	Instantaneous Temperature Profiles Perpendicular to Weld Line at 170 mm/min	52
4.3.3	Instantaneous Temperature Profiles Perpendicular to Weld Line at 200 mm/min	52
4.3.4	Variation of Temperature on Top Surface for Different Tool Travel Rates	53
4.4.1	Top Surface Temperature Contours after 2 Sec at Tool Travel Rate of 140 mm/min.....	55
4.4.2	Top Surface Temperature Contours after 38 Sec at Tool Travel Rate of 140 mm/min....	56
4.4.3	Top Surface Temperature Contours after 80 Sec at Tool Travel Rate of 140 mm/min....	56
4.4.4	Cross-Sectional View of Temperature Contours Through the Weld Seam	57
4.4.5	Instantaneous Temperature Profiles Perpendicular to Weld Line at 140 mm/min	57
4.4.6	Instantaneous Temperature Profiles Perpendicular to Weld Line at 180 mm/min	58
4.4.7	Instantaneous Temperature Profiles Perpendicular to Weld Line at 220 mm/min	58
4.5.1	Instantaneous Temperature Profiles Perpendicular to Weld Line at 100 mm/min	60

4.5.2	Instantaneous Temperature Profiles Perpendicular to Weld Line at 140 mm/min	60
4.5.3	Instantaneous Temperature Profiles Perpendicular to Weld Line at 180 mm/min	61
4.6.1	Instantaneous Temperature Profiles Perpendicular to Weld Line at 100 mm/min	62
4.6.2	Instantaneous Temperature Profiles Perpendicular to Weld Line at 125 mm/min	63
4.6.3	Instantaneous Temperature Profiles Perpendicular to Weld Line at 150 mm/min	63
4.7	Comparison between Rotational Tool Velocity and Tool Travel Rate for Al2024-T3	65

CHAPTER 1

INTRODUCTION

1.1 Background

Friction Stir Welding (FSW), patented by The Welding Institute [2] in 1991, is a new technique for material joining and processing. Friction Stir Welding is a solid-state welding technology that has been a very comprehensive method for joining non-ferrous materials such as aluminum alloys and copper. It is a solid-state process, occurring below the solidus temperature of the metals being joined. FSW produces welds that are high in quality, strength, and also inexpensive to make. The other main advantage is that it produces no fumes during process and is energy efficient. FSW does not need any filler material as required in conventional welding process and is relatively easy to perform. However, the workpiece should be rigidly clamped and welding speeds are low in order to avoid defects like porosity. For aluminium alloys such as the 2000, 5000, 6000, 7000, and 8000 series, the alloys can be easily welded by friction stir welding.

During FSW, the work piece is placed on a backup plate and is clamped rigidly to eliminate any degrees of freedom. A cylindrical tool with a pin normally one-third the diameter of the shoulder at the base of the shoulder rotates with a high speed in the range of 300 to 1000 rpm. It is slowly plunged into the work piece until there is contact between the shoulder surface and the work piece which consequently creates heat. The heat is consequently produced due to friction and the plastic deformation of the material. The tool then moves along the designated path on the workpiece with a specified travel rate. The pin of the rotating tool hence provides the “stir” action in the material of the work piece. This results in a Heat Affected Zone (HAZ) with a better grain refinement required for a good weld joining.

One of the main process parameters in FSW is the heat flux. The heat flux should be high enough to keep the maximum temperature in the work piece around 80% to 90% of the melting temperature of the work piece material [1], so that welding defects are avoided. The amount of the heat conducted into the work piece usually generates a good weld in terms of the microstructure of the Heat Affected Zone (HAZ), the residual stress, and the distortion of the work piece. Also the amount of the heat conducted back into the tool dictates the life of the tool. A low amount of heat transfer could lead to breakage of the pin due to its hard material. These factors emphasize the importance of the heat transfer aspect of friction stir welding.

1.2 Types of FSW

FSW when invented was intended to be used for simple butt welds. Over the years through rigorous testing and research it's being utilized for different types of joining processes. It is usually used to make three different types of weld joints – butt joints, lap joints, and spot welds.

1.2.1 Butt Joint

A butt joint is the most common type of weld obtained through the FSW process. For this type of joint the workpieces are held tight with adjoining edges against each other. The rotating tool at a constant rotational and translation velocity with sufficient downward force is moved across the workpiece surface. The friction between the shoulder and workpiece surface and the plastic deformation of the weld metal generates enough heat required to create the weld. The quality of weld depends on parameters such as the downward force on the tool, rotational speed of tool and travel rate of tool. Figure 1.1 shows the schematic representation of FSW of a butt joint.

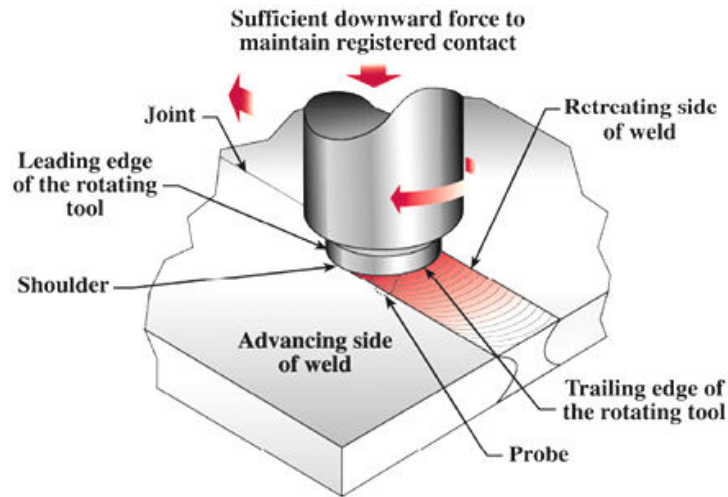


Figure 1.1. Schematic representation of FSW of a butt joint [2].

1.2.2 Lap Joint

The procedure for creating lap joints is similar to that of a butt weld with only difference being that the plates are placed one over the other. Hence there is an additional complexity related to the actual heat transfer between the two sheets. The tool used for lap joints has a longer pin than that used for a butt joint since it has to penetrate both the sheets for proper stirring action. Like butt joint FSW joining, process parameters such as tool pressure and the type of workpiece clamping fixture play a very important role in the quality of weld obtained [14]. In the case of lap joint FSW weld, the more the air gap the less the quality of weld obtained and vice versa. Figure 1.2 shows the schematic of the overlap configuration of a lap joint.

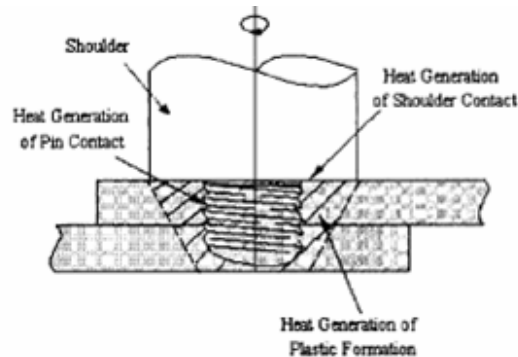


Figure 1.2. Schematic of an overlap FSW configuration [3].

1.2.3 Spot Weld

A FSW spot weld involves a process similar to FSW of a lap joint, but the difference being instead of moving the tool along the weld seam, the tool only presses the parts, which are placed on top of each other as illustrated in Figure 1.3

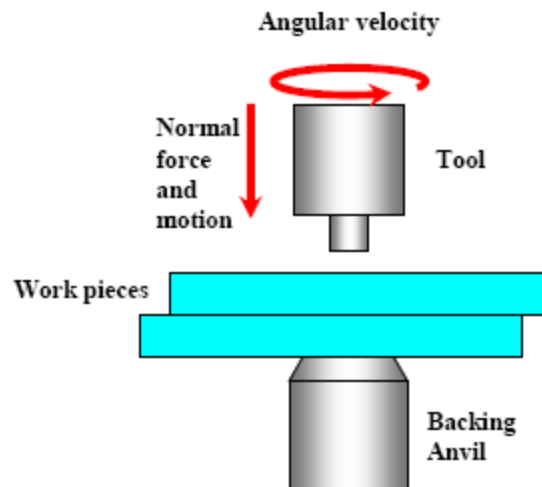


Figure 1.3. Schematic of a friction stir spot welding process [4]

1.3 Advantages and Disadvantages

The main advantage of FSW over traditional welding processes is the fact that no melting of the workpiece material is involved hence eliminating workpiece material and tool material loss. A few of the other advantages of FSW include:

- Defects like porosity and voids are less due to absence of material melting
- Low distortion and residual stresses in resultant welded zone
- Higher mechanical properties
- Absence of toxic fumes and radiation make it a very environmentally safe process

There are a few disadvantages associated with FSW process:

- Clamping of the workpiece is a very important criteria in the process
- Weld speeds are slower which can lead to longer process times

- Surface thickness is reduced marginally during the process as no filler material involved

1.4 Applications

Applications [2] of the FSW include various industries including few of the following:

- Shipbuilding and Marine Industries

FSW is suitable for many applications under shipbuilding such as manufacturing of hulls, panels for decks, aluminium extrusions, offshore accommodation, etc.

- Aerospace Industry

Most of the aerospace industries currently are welding mainly prototype and production parts by FSW. Longitudinal butt welds in Al alloy fuel tanks for space vehicles have been friction stir welded and successfully used. FSW could also be used to increase the size of commercially available sheets by welding them before forming. Other applications include manufacture of wings, fuselages, etc.

- Railway Industry

Most of the applications of FSW in railway industries include building of container bodies, railway tankers, etc.

- Land Transportation

FSW is currently being used by many automotive companies for various applications that include but not limited to building of engine chassis, wheel rims, truck bodies, mobile cranes, body frames, etc.

1.5 Problem Statement

The problem in incorporating FSW into manufacturing is that developmental process and testing is expensive from the view point of time, materials, and manpower. Much of the process knowledge is through running experiments for various changes in process parameters and then

looking at the resulting metallurgical aspects to analyze the results. This consequently slows down the development of applications for this process. A faster and more cost effective way to examine new aspects regarding friction stir welding is required to reduce actual experimental testing. Finite element modeling is an option which can help determine process parameters that require further experimental testing for validation and analysis. The post-weld microstructure depends largely on how the material is heated, cooled and deformed. Hence a prior knowledge of the temperature evolution within the workpiece would help in design of process parameters for a welding application. Research in the field of FSW lap joints has been limited possibly due to proprietary publishing restriction within industry. Hence it would be very beneficial for future development of FSW to understand the process behind FSW of lap joints by the means of Finite Element Analysis (FEA). Two process parameters of interest for FSW lap welds are tool travel rates and rotational tool velocities. A lot of emphasis has been laid on FEA analysis in previous published papers [3, 4, 6, 7, and 8] hence FEA analysis of these process parameters would broaden the scope of application of FSW lap welds.

1.6 Study Objectives

The main objectives of this study was to develop and validate three-dimensional thermal models of friction stir welding for butt and lap joints for specific experimental cases and investigate the effect of varying several process parameters on weld temperature history. In order to better understand the process an initial detailed study into butt welds was performed. The developed models would be validated against the published experimental results. The best validated model was used to further perform parametric studies to predict thermal history and temperature distribution necessary for high quality welds. The parametric study was designed to investigate the following:

- Effects of various aluminium alloys such as Al6061-T6, Al5052-H32, AA7050-T451, and Al2024-T3 on workpiece temperature evolution.
- Effect of variation of tool travel rates and different workpiece materials on workpiece temperature evolution.
- Effect of variation of rotational tool velocity for FSW lap weld of Al2024-T3 alloy on workpiece temperature evolution.

Such process parameter studies covering parametric conditions not found in the literature would provide insights for further testing and analysis needed for development of process specifications for FSW butt and lap welds.

1.7 Methodology

The basic study methodology was to develop a computational thermal model for butt and lap welds based on published experimental data. The correlated model would be extrapolated to perform further parametric studies involving process conditions not seen in the research literature. The unique focus of the study was to investigate thermal modeling of FSW lap welding which has been less researched than butt welding. Commercial code LS-DYNA from Livermore Software Technology Corporation (LSTC) was FEA code used in the study. The geometric model was developed using a pre-processor MSC.Patran. The generated output LS-DYNA key file was modified to correlate the model with published experimental results. A mesh independence study was also performed to identify the effect of mesh density on the temperature evolution through the workpiece. The overall temperature evolution through the workpiece during welding process was observed through the generated temperature contour plots and temperature-time history plots.

CHAPTER 2

LITERATURE REVIEW

Development of the FSW process since 1991 has included various experimental investigations. Many investigations over the years have published numerous papers that dealt with different parametric studies related to thermal profiles during the FSW process. Only in the past few years have computational modeling methods for this process been more clearly understood. The typical approach for FSW modeling is to obtain numerical predictions and then compare and validate the results against experimental temperature measurements in workpiece through thermocouples. Various attempts have been made to understand the mechanism for heat generation using this methodology.

2.1 Thermal Process Models of FSW of Butt and Lap Welds

Gould and Feng [5] performed a 3-D analytical study to predict the workpiece temperatures for FSW butt weld using the Rosenthal equations describing a moving heat source. The heat input was a function of process parameters including tool rpm and force on tool and was directly applied on top of the workpiece with radius equal to that of the tool shoulder. Heurtier et al. [6] used an analytical model to predict workpiece temperatures but later it was converted to numerical analysis to increase prediction accuracy.

Tang et al. [7] focused their study to the FSW tool heat input and resulting temperature distribution during FSW butt weld. They found that the maximum temperature in the weldline was below 80% of melting point of Al6061-T6. It was also found that temperature distribution perpendicular to the weld was isothermal under the pin shoulder, and increasing welding pressure and pin tool rotational speed increased the peak temperature.

One of the first numerical FSW studies was produced by Chao and Qi [8]. In their research temperature fields during welding, the residual stress distribution and distortion of workpiece after FSW were studied. A de-coupled heat transfer and thermo-mechanical modeling and analysis and three-dimensional finite element formulation was used in their study. Also a moving heat source with heat distribution simulating the heat generated from friction between tool shoulder and workpiece was implemented as the heat input.

The main sources of heat were from friction between tool shoulder and workpiece and from the plastic deformation of weld material in vicinity of rotating pin. The empirical equation for calculating the heat input in their analysis is given by equation (1.0).

$$q(r) = \frac{3Q_3 r}{2\pi r_o^3} \quad \text{where } r \leq r_o \quad (1.0)$$

where $q(r)$ is the rate of heat flux, Q_3 is the heat flux to shoulder.

A trial and error approach was used wherein the total heat input to workpiece and heat convection coefficient of bottom surface are calculated by fitting the measured temperature data with the analytical model. This was also known as the inverse approach. These temperatures were then used to determine the residual stress after the FSW process. The results matched to a greater extent and the process was comparatively simpler than the direct approach used by various other authors. According to the authors approximately 95% of the heat generated from friction was transferred to workpiece and the remaining 5% was transferred to the tool. The fraction of rate of plastic work dissipated as heat was approximately equal to 80%. Figure 2.1 shows the schematic representation of the applied boundary conditions in the model used by Chao and Qi.

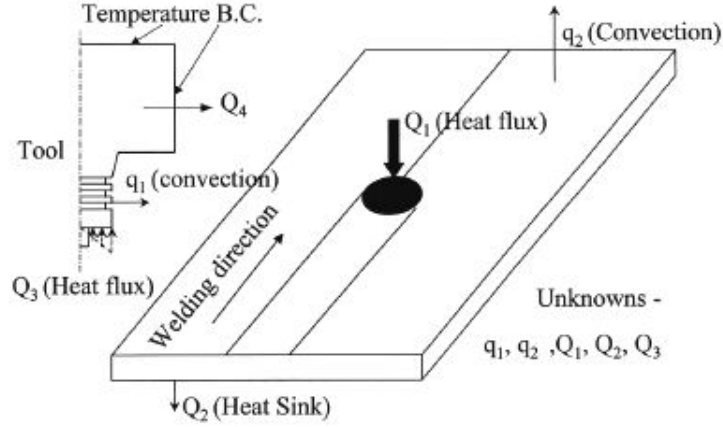


Figure 2.1. Schematic representation of boundary conditions [8].

Colegrove et al. [9] in 2000 published their finite element thermal model development for FSW process. Their model included the backing plate and the tool. Their goal was to predict the material flow patterns around the tool. For the heat input they followed an iterative method to have a proper validation between the experimental and predicted values.

Zhu and Chao [10] in their study investigated the effect of each temperature-dependent material property on the transient temperature, residual stress and distortion in the finite element simulation of FSW butt weld process. Their analysis methodology suggested using an approach based on properties characterized by a linear function for the temperature at yield stress and constant room-temperature values for other remaining properties.

Song et al. [11] developed a three dimensional transient model for a FSW butt weld. In their research the plastic heat generation near the pin region was modeled as the heat source. Also transient heat transfer at the tool pin penetrating and pulling up condition was considered in the study. An explicit central differential scheme was used to solve the control equations in process. Tool shoulder/workpiece boundary condition was a Neumann or heat flux boundary condition and was calculated from frictional heat. Also a convective boundary condition was also applied to the back plate to account for the heat transfer through the bottom surface of the sheets

to the backup plate. As the contact resistance between the sheet and backup plate was not known this assumption was made. For the tool pin boundary condition, heat generation was considered to be a uniform volumetric heat generation source near pin region and is linear to pin rotational speed which was given by equation (1.1) where ω is the tool rotational speed, K_s is the arbitrary constant. With all units being defined in metric system.

$$S = K_s \omega \quad (1.1)$$

Heat input to tool shoulder in FSW is calculated from frictional heat between tool and workpiece. Equations (1.2) and (1.3) were used to calculate the heat input.

Torque to rotate tool,

$$M = \frac{2}{3} \mu \pi P (R_o^3 - R_i^3) \quad (1.2)$$

Heat exerted to workpiece,

$$Q_o = \frac{4}{3} \mu \pi^2 P n (R_o^3 - R_i^3) \quad (1.3)$$

In equation (1.3), $\mu = -0.00027T + 0.581$, P is pressure on tool and n is tool rotational speed.

Ahmed et al. [12] in their research performed a computational and experimental study of high speed FSW butt weld. The model used for the computational study was a heat source model moving along the butt weld line. For thermal modeling, three sources of heat were considered, frictional heat generated at interface of shoulder and workpiece, frictional heat at pin contact and plastic deformation of welded metal. Heat generated depended mostly on the plunging tool force and tool travel rate. The total heat input Q (in watts) was calculated by equation (2.0),

$$Q = (4/3) \mu(T) p(T) \pi^2 \omega (R_o^3 - R_i^3) \quad (2.0)$$

where $\mu(t)$ is the friction coefficient between tool and workpiece, ω is the rotational speed, and $p(t)$ is the pressure on shoulder of tool.

A convective thermal condition was applied with a coefficient of 30W/m²C on top surfaces of both the workpieces with ambient temperature at 28°C. Radiation losses were considered with ambient temperature of 28°C while the contact conductance between bottom surface of workpiece and back-plate taken negligibly small or neglected. Results were validated with experimental results obtained through infrared camera and thermocouples. They found that for Al6061-T6 sound welds were obtained between 570-530°C surface temp and spindle velocities of 125mm/min and 250mm/min.

Khandkar et al. [13] presented an input torque based thermal model for FSW of Al6061-T6 alloy. Their objective was to predict thermal history and temperature distribution during FSW for a butt joint. In their study the moving heat source represented by the heat generated by tool rotation and linear traverse of the shoulder and pin has been correlated to the torque data obtained from experimental data. The heat is mainly due to surfaces of the tool making contact with the workpiece. The equation (2.1) to equation (2.4) was used:

$$M = \int_{r_i}^{r_o} (\tau r)(2\pi r) dr \quad (2.1)$$

where M is the torque at shoulder, r is the tool radii; τ is the torsional shear stress.

$$\tau = \frac{Mr}{J} \quad (2.2)$$

Torque was related to average power input by the equation (2.3),

$$P_{av} = M_{tot} \omega \quad (2.3)$$

where P_{av} is the average pressure on tool, ω is the rotational speed of tool.

The finite element heat flux is related to radial position of tool shoulder by equation (2.4),

$$q(r) = \omega \tau r = 2\pi N \tau r \quad (2.4)$$

where N is the tool rotation speed in rps, τ is the shear stress.

Khandkar and Khan [14] presented a thermal model for overlap joints using FSW in their research paper. Their paper deals with a 3D thermal model to predict temperature distribution in overlap joints. The model accounted for moving heat generation caused by friction at the interface between tool shoulder and workpiece and the friction between pin and workpiece. The results were validated using experimental results for 5454-O Al alloy.

For the energy equation, an unsteady heat flow was modeled as a 3D problem. Transient heat flow within workpiece is given by equation (2.5),

$$\frac{\partial(\rho c T)}{\partial t} + \nabla \cdot (\rho c \vec{V} T) = \nabla \cdot (k \nabla T) + q \quad (2.5)$$

where q is the moving heat generation/unit vol.

Heat is generated by rotating tool and motion of weld metal relative to tool and the sources were due to friction of shoulder and workpiece given by equation (2.6), and due to friction of pin and workpiece given by equation (2.7).

$$q_{\text{shoulder}} = \frac{2\mu F N r}{r_{\text{shoulder}}^2 - r_{\text{pin}}^2} \quad (2.6)$$

where r = distance from moving center of shoulder, F is the downward force on tool.

$$q_{\text{pin}} = k_1 \frac{2\mu F N r}{r_{\text{shoulder}}^2 - r_{\text{pin}}^2}, \quad \text{where } k_1 = 3\% \quad (2.7)$$

For the Boundary Conditions (B.C) the authors used Newtonian boundary conditions (equating the Fourier law temperature gradient at the surface to the heat flux) at left and right sides of top and bottom sheets given by equation (2.8).

$$-k \left. \frac{\partial T}{\partial x} \right|_{\text{Left/Right}} = \alpha_{\infty} (T - T_{\infty}) \quad (2.8)$$

where α_{∞} is the ambient convective coefficient, k is the thermal conductivity.

Also Newtonian boundary conditions were applied at front and rear ends of top/bottom sheets,

$$-k \frac{\partial T}{\partial z} \Big|_{\text{Front/Rear}} = \alpha_{\infty} (T - T_{\infty}) \quad (2.9)$$

The B.C for top surface of top sheet given by equation (2.10),

$$-k \frac{\partial T}{\partial y} \Big|_{\text{Top}} = \alpha_{\infty} (T - T_{\infty}) \quad (2.10)$$

B.C for bottom surface of bottom sheet given by equation (2.11),

$$-k \frac{\partial T}{\partial y} \Big|_{\text{Bottom}} = \alpha_{\infty} (T - T_{\infty}) \quad (2.11)$$

Also the thermal contact in between the faying surfaces of the two sheets was defined by equation (2.12).

$$HTC = HTC_0 * p \quad (2.12)$$

where HTC = heat transfer coefficient, p = pressure distribution at faying surface.

The surface contact conductance between the two sheets was modeled related to varying pressure with highest pressure being directly applied below the shoulder area and gradually decreasing outwards. Their model provided good match between experimental and predicted results. This is currently the only published research data related to overlap FSW and hence would be the main source of information for this study.

2.2 FSW Process Parameters

Based on research review, the main process parameters for FSW could be summarized as below:

- Welding forces during the process:

Forces like a downward force, traverse force and a lateral force may act on the tool required in order to achieve the best welding cycle.

- Design of the tool:

It is necessary that the tool is strong enough throughout the weld temperature. Hence various tool designs have been proposed in the past years for better weld quality and tool life. Most of the tools used today have concave shoulder that helps in preventing material from extruding out from sides of tool shoulder.

- Angle of tool tilt and plunge depth:

The angle of tilt around 2-4 degrees is usually adopted in various FSW processes. It helps in a proper forging process. The plunge depth into the workpiece increases the pressure below the tool and provides good forging of material behind the tool.

- Tool traverse and rotational speeds:

From various studies it has been concluded that by increasing the rotation speed of the tool and decreasing the traverse speed of the tool the temperature in the weld region increases. Adequate temperature is necessary because if the material is too cold then voids may form and if the material is too hot then it could lead to defects due to the liquation of low-melting point phases.

- Heat generation:

The welding cycle can generally be classified into 4 stages

Dwell: Here the material is preheated by stationary rotating tool.

Transient heating: When tool moves a transient state is reached where temperature begins to change with time until steady state is reached.

Pseudo steady state: Here the thermal state remains constant.

Post steady state: Here heat may reflect from end of plate causing tool to overheat.

CHAPTER 3

METHODOLOGY

The basic methodology was to develop a model based on vital points summarized from different published papers as discussed in literature review. The finite element model would be correlated with published experimental data. The best correlated model would be extrapolated to perform further parametric studies involving butt and lap welds. Commercial code LS-DYNA by LSTC was the FEA code used in the study. The geometric model was developed using a pre-processor MSC.Patran. The parametric study was performed by varying the tool travel rates and rotational tool velocities and observing the overall temperature evolution through the workpiece during the welding process. This was facilitated by the generation of temperature contour plots and temperature-time history plots for various cases of butt welds and lap welds.

3.1 Introduction to MSC.Patran 2005

Companies today are increasingly using computer aided design and analysis to reduce expensive physical modeling and testing. MSC.Patran [15] enables us to develop and test a product using computer-based simulation prior to making any manufacturing and material designs. Through MSC.Patran, finite element models can be created from various computer-aided design (CAD) parts which could be submitted for simulation to visualize the simulated model behavior. These results can then be used to improve the product designs for reduced material usage and higher performance.

The benefits of CAD modeling include:

- Cost reduction through replacing physical experiments with less expensive simulations
- Customize modeling environment to enhance simulation process

Applications of the software include:

- Aerospace
- Automotive
- Ship Building
- Medical Products
- Consumer Products

Different meshing styles are available in MSC.Patran ranging from fully automatic solid meshing to detailed node and element editing. Flexible options are available for application of loads and boundary conditions to the analysis model. It uses a customized interface for different solvers through MSC's unique preference options. These options are available for MSC.Nastran, and other analysis solvers like ABAQUS by Abaqus Inc, LS-DYNA by LSTC, ANSYS, etc. The MSC.Patran library source includes solvers for structural analysis, advanced structural analysis, thermal analysis, fatigue simulation and composite laminate modeling. In this study MSC.Patran 2005 is used for the purpose of pre-processing of computational models. The initial geometry and mesh creation, constraints and contact surfaces are defined with the help of a Graphical User Interface (GUI) included in MSC.Patran.

3.2 Introduction to LS-DYNA

LS-DYNA [16] is a general purpose finite element code released by LSTC (Livermore Software Technology Corporation) for transient dynamic analysis capable of simulating complex real world problems. The basic methodology is based on explicit time integration. There is also an implicit solver available for purpose of heat transfer analysis.

Significant features of LS-DYNA include:

- Fully automatic definition of contact areas

- Large library of constitutive models
- Large library of element types
- Special implementation for the automotive industry (seatbelt, airbag, dummy)
- Special features for metal forming applications (adaptive mesh)

Beside the explicit solver, the following solvers are also available:

- Different implicit solvers
- Arbitrary Lagrangian Eulerian (ALE)
- Thermal solver (*used in this study*)
- Coupled fluid dynamics (CFD)
- Smooth Particle Hydrodynamics (SPH)

3.2.1 File Structure

A classic LS-DYNA data file must contain:

- final time
- material description
- geometry description
- list of nodes with coordinates and constraints
- list of elements with connectivity
- forces, velocity conditions, contact interface

3.2.2 LS-DYNA Thermal Weld Model

The exact interaction between the heat source and the weld model is a complex phenomenon that cannot be modeled with ease. A weld heat source model by J. Goldak [17] is used by LS-DYNA to model the weld heat source. This model is based on the Gaussian distribution of power in space. An important feature of this model is that it uses a double

ellipsoidal method of heat deposition such that the size and shape of the energy source can be easily changed to account for different types of welds namely, arc welding, laser and beam welding, and friction stir welding. Figure 3.2 shows the Goldak's model.

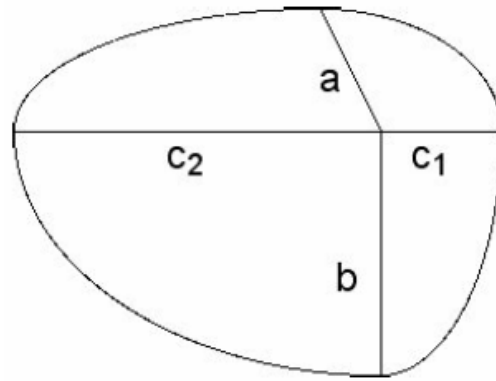


Figure 3.2. J. Goldak's heat source model [17]

The weld shape parameters (a , b , C_1 , C_2) are defined by using the `BOUNDARY_THERMAL_WELD` keyword in the LS-DYNA input file.

3.3 LS-PREPOST

LS-PREPOST [16] is a new post processor for LSDYNA developed by LSTC. It is a full featured post-processor for all types of LS-DYNA simulations. The graphic user interface is designed in a manner to create a user friendly environment. It supports the latest Open-GL standards to provide fast rendering for fringe plots and animation results. It also handles the ASCII output data and links it to the input files and animations.

A few of LS-PREPOST features include:

- Contour plots
- X-Y graphs
- Overlay plots
- Vector plots
- Animations

- Multiple view ports
- ASCII plotting
- Printing formats: PS, TIFF, PNG, JPG, VRML, GIF
- Movie formats: MPEG, AVI
- Input deck manipulation
- Mesh manipulation

3.4 Model Development for FSW of a Butt Weld

3.4.1 Geometry

The geometric modeler used in this study is MSC.Patran. Two sheets are modeled with each sheet having dimensions of 0.305m*0.105m*0.008m. Figure 3.4 shows the modeled geometry.

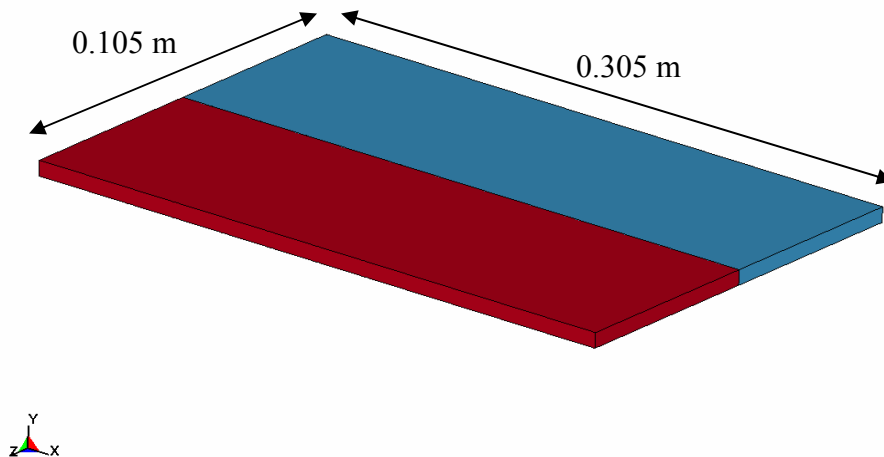


Figure 3.4. Geometric model of two plates to be welded.

3.4.2 Mesh Development

The two sheets were meshed with the same mesh parameters and elements. Three dimensional solid quad elements were used to mesh the sheets. A total of 20000 elements (250

by 20 by 4 grid-points along the length, width and thickness of each sheet respectively) are generated in each sheet with mesh density being fine at the weld line and gradually increasing in coarseness away from the weld line. Figure 3.5 shows the finite model of the sheets.



Figure 3.5. Finite element model of the sheets.

3.4.5 Material Properties

Three different alloys were used in the butt weld study, Al6061-T6, Al5052-H32, and AA7050-T7451. Their properties are tabulated in Tables 3.1, 3.2, and 3.3 respectively while Figure 3.6 shows the comparison of thermal properties for different Aluminium alloys obtained from data collected from ASM handbook and published papers. The temperature dependent properties were included in LS-DYNA models for butt and lap welds.

Table 3.1

Thermal material properties of Al6061-T6 alloy [13]

Temperature °C	-17.8	37.8	148.9	204.4	260	371.1	426.7	582
Specific heat J/Kg °C	904	945	1004	1028	1052	1104	1133	1230
Thermal Conductivity W/m °C	162	162	184	192	201	217	223	253

Table 3.2

Thermal material properties of Al5052-H32 alloy [10]

Temperature °C	0	80	180	280	380	480	520	590
Specific heat J/Kg °C	900	960	1000	1050	1100	1150	1155	1200
Thermal Conductivity W/m °C	160	170	185	205	220	230	235	250

Table 3.3

Thermal material properties of AA7050-T7451 alloy [18]

Temperature °C	20	100	200	300	400	510
Specific heat J/Kg °C	866	915	949	1041	1178	1276
Thermal Conductivity W/m °C	135.42	165.79	185.18	207.06	222.43	220.14

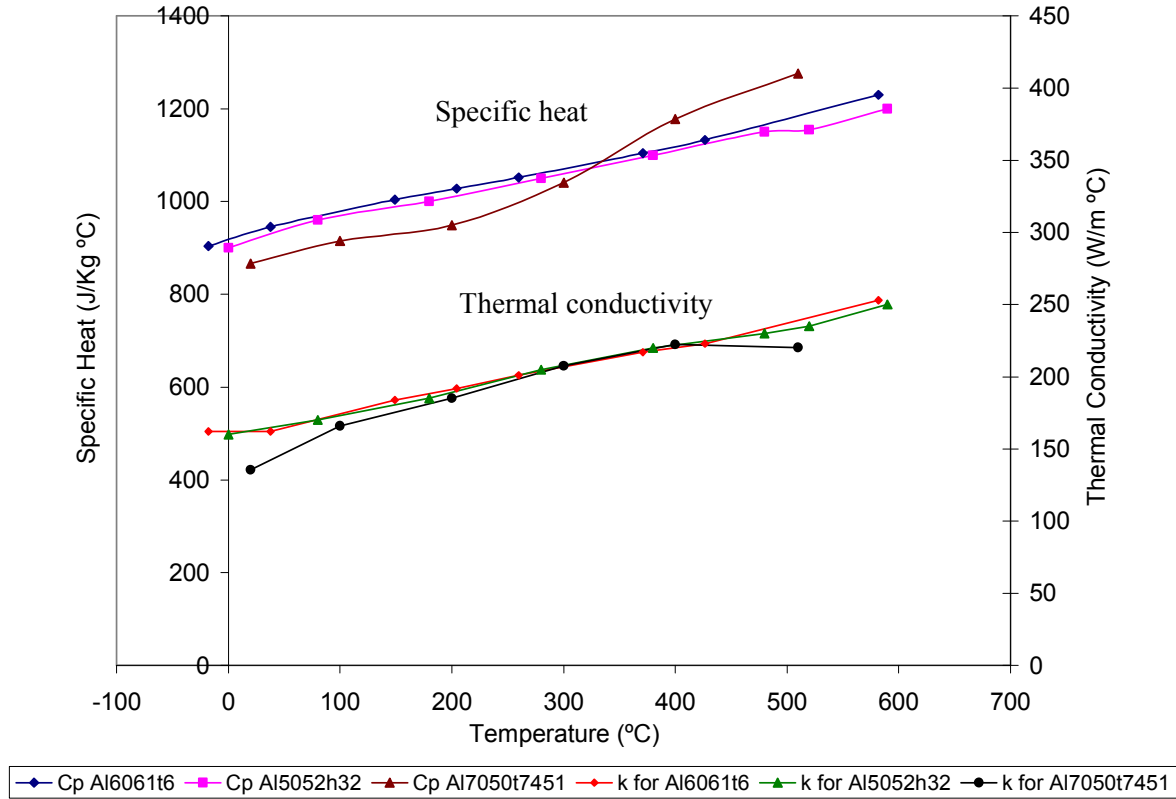


Figure 3.6. Comparison of thermal properties for different Aluminium alloys.

3.4.4 Boundary Conditions

Boundary conditions for the butt weld model were specified through LS-DYNA codes. Assumptions were made for various boundary conditions based on data collected from various published research papers [1, 10, 12, and 13]. The boundary conditions in this model are usually dependent on the overall heat transfer process.

Convective heat losses occur across all the free surfaces of the work piece and conduction losses occur from the workpiece surface to the backup plate. Also there is a small heat loss to the tool and minimal heat loss through radiation from the workpiece surface. As the difference in process temperatures and ambient temperatures are relatively low, the percentage of heat lost due to radiation is low (less than 3% according to Khandkar et al.). Hence the effective radiative heat losses were neglected.

Convective boundary conditions for this process are defined at the free surfaces i.e., top and side surfaces of the sheet by equation (3.6).

$$-k \frac{\partial T}{\partial n} \Big|_{\text{free_surfaces}} = h_{\infty} (T - T_{\infty}) \quad (3.6)$$

Parameter n represents the direction coordinate, h_{∞} is the ambient convection coefficient, k is the thermal conductivity of the sheet and T_{∞} is the ambient temperature. In this current model a typical value of h was taken to be $15 \text{ W/m}^2 \text{ }^{\circ}\text{C}$ using an ambient temperature of 22°C for top and side surfaces of workpiece as this is typical for FSW heated top surfaces [13,14].

In order to account for the conductive heat loss through the bottom surface of weld plates a high overall heat transfer coefficient has been assumed off the bottom surface of sheets similar to the researcher's work [8] as discussed in literature review. This factor simplified as pseudo-convective Newtonian boundary condition [3] is described as in equation (3.7).

$$-k \frac{\partial T}{\partial y} \Big|_{\text{bottom}} = h(T - T_{\infty}) \quad (3.7)$$

where h is the simplified convective coefficient at bottom surface of the sheets in contact with the backup plate. Due to the complexity involved in obtaining the contact condition between the sheet and backup plate, the value for h had to be estimated by assuming different values through reverse engineering technique. In this study the optimized value for h was found to be $300 \text{ W/m}^2 \text{ }^{\circ}\text{C}$.

Figure 3.7 shows the schematic representation of boundary conditions that were used for the FSW of the butt weld model.

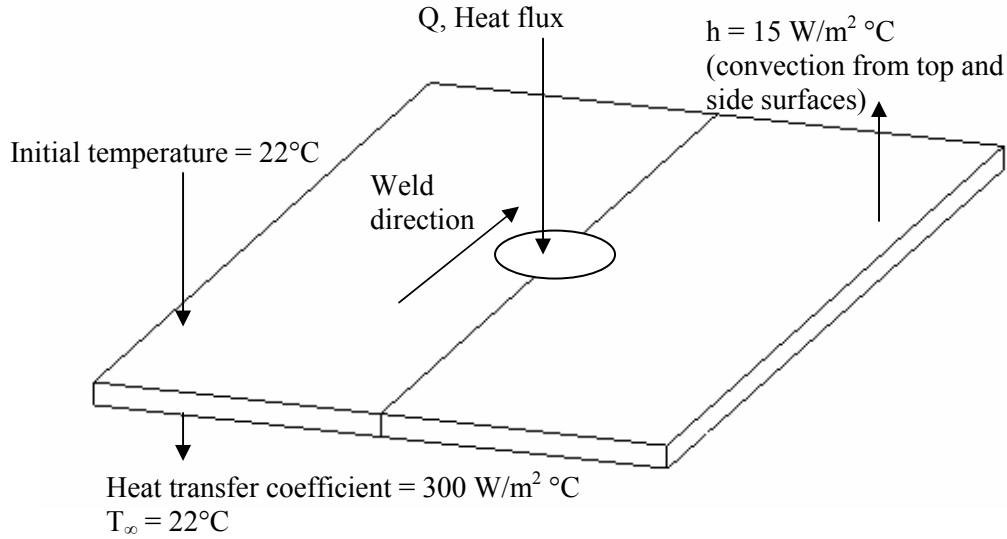


Figure 3.7. Schematic representation of boundary conditions for FSW of butt weld.

3.4.5 Heat Input Implementation for Butt Weld

The heat generated in the FSW process is due to the following [19] main factors:

- Frictional heat at the interface of the shoulder and the workpiece
- Plastic deformation of the weld metal in the area surrounding the pin

The heat generated by plastic deformation of the weld metal in the area surrounding the pin is of a lower magnitude [8] and is difficult to quantify. Hence it was neglected in this study. Therefore in this model, only the heat generated by friction between the workpiece and tool shoulder was considered.

The total heat transfer process in the workpiece is transient compared to a relatively steady state heat transfer process using a tool frame of reference. Total heat input to the workpiece calculated through the empirical equation is applied on the shoulder area to predict the overall temperature evolution in the workpiece.

The total heat input Q in watts for this model is calculated through Frigaard et al. [20] equation and is applied as a moving heat source through LS-DYNA code that uses Goldak's

moving heat source model rather than using Rosenthal's moving heat source model used by various researchers [5, 7]. The torque required to rotate a circular shaft relative to the plate surface under the action of axial load is given by equation (3.1),

$$M = 2/3 \mu \pi p(r) R^3 \quad (3.1)$$

Where M is the torque, μ is the dynamic friction coefficient, R is the surface radius and $p(r)$ is the pressure distribution across the interface between tool and workpiece with all units being in S.I. system.

$$Q = \int_0^R \omega dm \quad (3.2)$$

$$Q = \int_0^R \omega 2\pi \mu p r^2 dr \quad (3.3)$$

Where Q in equation 3.3 is the total heat generated, p is the pressure of the shoulder on to the workpiece and ω is the angular velocity. Substituting $\omega = 2\pi N$ in the equation (3.3) we have,

$$Q = \int_0^R 4\pi^2 \mu p N r^2 dr \quad (3.4)$$

$$Q = \frac{4}{3} \mu p \pi^2 N R^3 \quad (3.5)$$

Therefore by equation (3.5), the rate of heat generation at the interface between the shoulder and top of the workpiece surface is a function of the frictional coefficient $\mu(T)$, rotational velocity N (rotations per second), and radius of shoulder R .

The tool shoulder radius used in this butt weld study was 12.5 mm, tool pin radius was 5 mm and the tool pin length was 8 mm. The dimensions for the tool were obtained from Khandkar et al. [13] for correlation to the published research data. The dynamic friction coefficient, μ is a complex factor and is a function of various parameters such as temperature,

surface roughness, travel rate of tool and the pressure applied [11]. Hence in order to evaluate the frictional coefficient an inverse approach was adopted. Two simulation runs were performed where the heat input value was used to back calculate the friction coefficient while in the second simulation the overall peak temperatures were used to calculate the friction coefficient. Through a trial-error procedure a frictional coefficient of 0.3 to 0.4 was found to give comparable results. The frictional coefficient range was similar to that used by other researcher's [1, 3, 8, 13]

3.5 Model Development for FSW of a Lap Weld

3.5.1 Geometry

The geometric modeler used in this study is MSC.Patran 2005. Two sheets are modeled with each sheet having dimensions of 0.305 m long by 0.102 m wide by 0.0018 m thick. Figure 3.8 shows the modeled geometry. The dimensions of the model for the butt and lap weld are similar except the thickness which is lower for sheet used for lap weld.

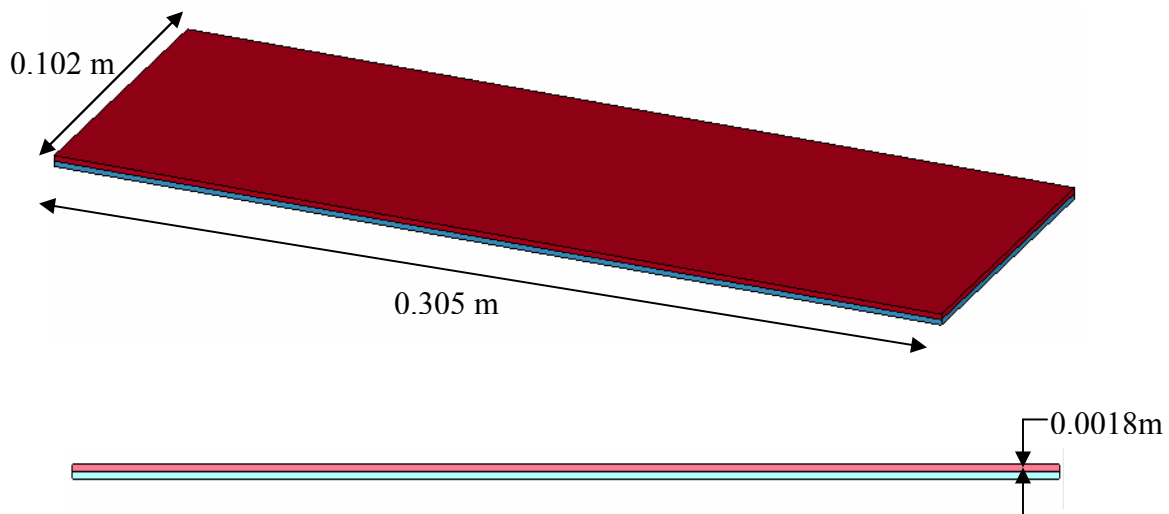


Figure 3.8. MSC.Patran model of two sheets lapped over each other (Isometric view and side view of two sheets).

3.5.2 Mesh Development

The two sheets were meshed with the same mesh parameters and elements, consisting of three dimensional solid quad elements. A mesh independency study was done to check for the effect of mesh density on the results. From mesh independency check the results for the model having 15000 elements and more were similar hence the model with 15000 elements was chosen for reduced computational time. A total of 250 by 20 by 3 grid-points or elements were generated in each sheet along the length, width and thickness respectively. A variable mesh density was used along the width of sheets such that it was finer towards the weld line while coarser towards the edge of the sheet with the smallest element being 1 mm at that region. Figure 3.9 shows the meshed sheets.

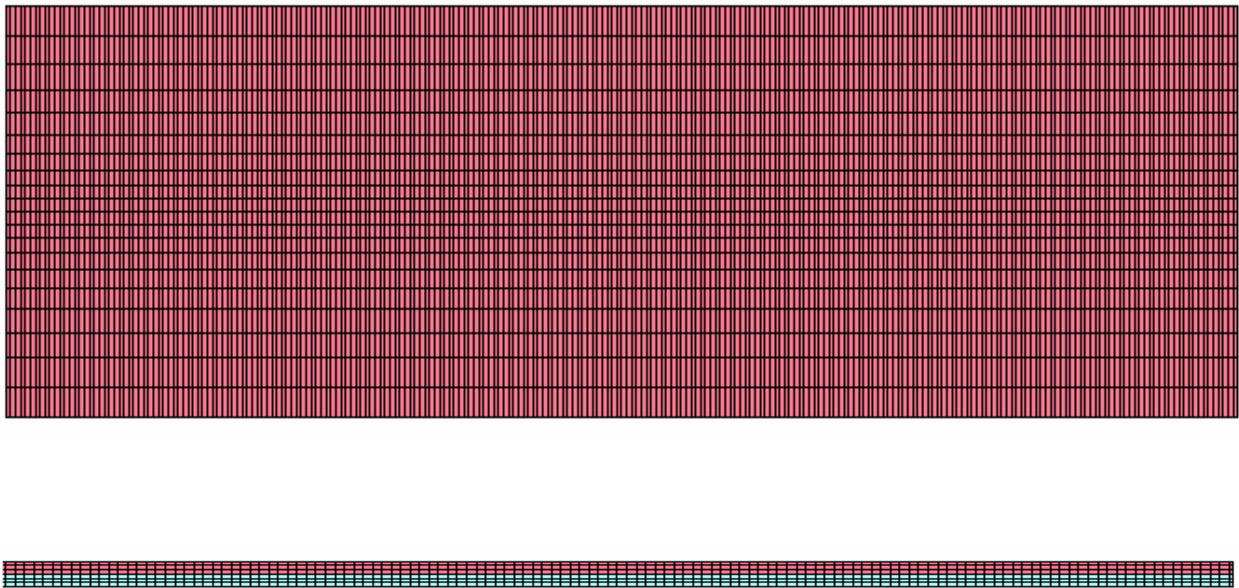


Figure 3.9. Finite element model of the two sheets lapped together (Top view and side view).

3.5.3 Material Properties

Three different alloys were used in this lap weld study: Al6061-T6, AA7050-T7451, and Al2024-T3. Their properties are tabulated in Tables 3.1, 3.3, and 3.4 respectively. The material properties were obtained from published data and ASM Handbook [13, 18, 14, and 24].

Table 3.4

Thermal material properties for Al2024-T3 alloy [14]

Temperature °C	20	100	200	300	400	500	545
Specific heat J/Kg°C	850	900	950	970	1000	1080	1100
Thermal Conductivity W/m °C	176	185	193	193	190	189	189

3.5.4 Boundary Conditions

Boundary conditions for the butt weld model were specified through LS-DYNA codes. Assumptions were made for these boundary conditions based on data collected from various published research papers [1, 10, 12, and 14].

Similar to the butt weld model, in the lap weld model the convective heat losses occur across all the free surfaces of the work piece and conduction losses occur from the workpiece surface to the backup plate. Also there is a small heat loss to the tool and minimal heat loss through radiation from the workpiece surface. As the difference in process temperatures and ambient temperatures are relatively low, the percentage of heat lost due to radiation is low (less than 3% according to Khandkar et al.) the effective radiative heat losses are neglected.

Convective boundary conditions for this process are defined at the free surfaces i.e., top and side surfaces of the sheet by equation (3.6).

$$-k \frac{\partial T}{\partial n} \Big|_{\text{free_surfaces}} = h_{\infty} (T - T_{\infty}) \quad (3.6)$$

In equation (3.6) n represents the direction coordinate, h_{∞} is the ambient convection coefficient, k is the thermal conductivity of the sheet and T_{∞} is the ambient temperature. In this current model

the value of h is taken to be $15 \text{ W/m}^2 \text{ }^\circ\text{C}$ for an ambient temperature of 25°C for both top and side surfaces of workpiece as its effect on the overall temperature history of the workpiece quite low as assumed by many researchers [8, 13, and 14].

As with butt weld simulation in order to account for the conductive heat loss through the bottom surface of weld plate a high overall heat transfer coefficient has been assumed off the bottom surface of the bottom sheet as done by researchers [3, 8, 12, 13] . This assumption was being made on the fact that the exact contact resistance between the sheet and plate is difficult to be accurately quantified. This factor simplified as pseudo- convective Newtonian boundary condition [14] is described as in equation (3.7).

$$-k \frac{\partial T}{\partial y} \bigg|_{\text{bottom}} = h(T - T_\infty) \quad (3.7)$$

In equation (3.7) h is the simplified convective coefficient at bottom surface of the sheet in contact with the backup plate. Due to non-availability of the contact condition between the sheet and backup plate the value for h had to be estimated by assuming different values [email correspondence Dr. Chao) through reverse engineering technique adopted by various researchers [3, 8, 12, and 13]. In this study the optimized value for h was found by back calculating the value necessary for correlating experimental peak temperatures with simulated peak temperatures. This value was found to be $150 \text{ W/m}^2 \text{ }^\circ\text{C}$.

For the boundary condition in between the two sheets, the contact condition is quite complicated to be calculated physically and also related experimental studies are limited in this area [14, 21]. This concept of Thermal Contact Conductance (TCC) has been obtained from the works of Xu and Khan [21] and Khandkar et al. [14]. As discussed in the literature review, they developed this concept because the contact resistance between the faying surfaces dictates the overall thermal history and this value is directly proportional to the pressure applied on the tool.

A relationship was developed between the basic heat transfer coefficient and a dimensionless contact pressure at the surfaces in contact given by equation (3.10). According to this equation the heat transfer coefficient increases with increasing pressure.

$$HTC = HTC_o * p \quad (3.10)$$

In equation (3.10) HTC is the heat transfer conductance and HTC_o is the basic thermal contact conductance in this case $2 \times 10^6 \text{ W/m}^2\text{°C}$ calculated for this study using an equation developed by Madhusudana [25] and p is the dimensionless pressure distribution factor.

In this study the TCC at areas below tool shoulder have been taken to be highest of $2 \times 10^6 \text{ W/m}^2\text{°C}$ while it decreased by a factor of 10 away from the tool shoulder region. This was to account for the rapidly decreasing tool pressure away from region below the tool shoulder and therefore contact resistance as predicted by equation (3.10). Different values for the (TCC) have been investigated for the model verification with cases having fixed TCC and variable TCC. Figure 3.10 shows the schematic representation of boundary conditions that were used for the FSW of lap weld model.

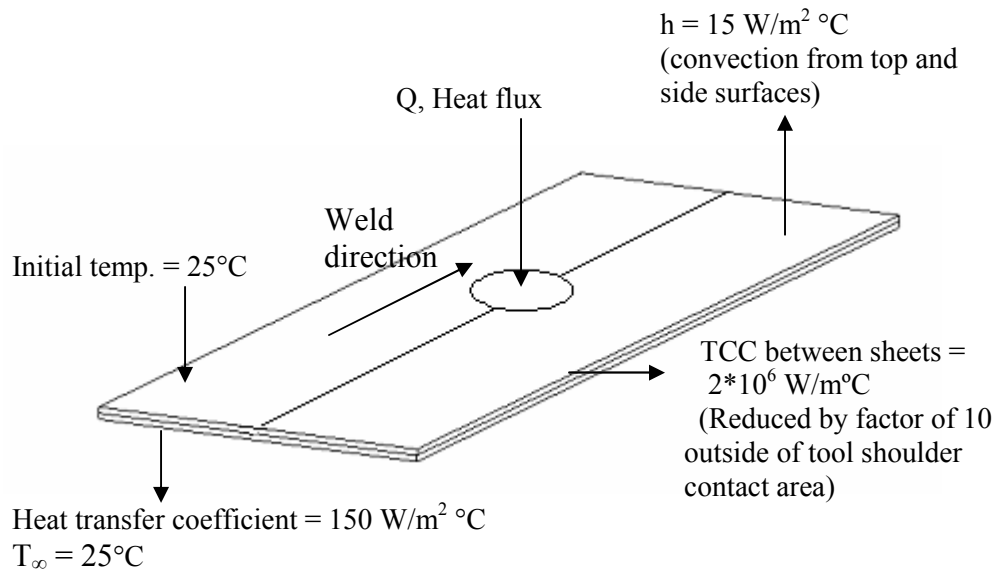


Figure 3.10. Schematic representation of boundary conditions for FSW of lap weld.

3.5.5 Heat Input Implementation for Lap Joint

Currently the heat generated process in FSW [14] was assumed to be similar to butt weld model due to lack of adequate information on lap welds. However in both the butt and lap welds, heat is generated by friction between the shoulder/pin and workpiece as well as through the plastic deformation of the workpiece material [8].

As with the butt weld, the heat generated by plastic deformation of the weld metal in the area surrounding the pin is of a significantly lower magnitude [8] and is difficult to be exactly quantified. Hence it was neglected in this lap weld study. Therefore in this model, only the heat generated by friction between the workpiece and tool shoulder was considered.

The total heat transfer process in the workpiece is transient from a workpiece frame of reference compared to a relatively steady state heat transfer process from a tool reference frame. Total heat input to the workpiece was calculated through the empirical equation (3.11) was applied on the shoulder area to predict the overall temperature evolution in the workpiece. The total heat input Q for this model was calculated through Frigaard et al. [20] equation (3.11)

$$Q = \frac{4}{3} \mu p \pi^2 N R^3 \quad (3.11)$$

The rate of heat generation at the interface between the shoulder and top of the workpiece surface is a function of the dynamic frictional coefficient μ (T), rotational velocity N , and radius of shoulder R . The tool shoulder radius used in this butt weld study was 12.5 mm, tool pin radius is 5 mm and tool pin length was 2.8 mm. The dimensions for the tool were obtained from Khandkar et al. [13] for correlation purposes. The dynamic friction coefficient, μ , is a complex factor and is a function of various parameters such as temperature, surface roughness, travel rate of tool and the pressure applied. Hence in order to evaluate the frictional coefficient an inverse approach was adopted. Two simulation runs were performed where the heat input value was used

to back calculate the friction coefficient while in the second simulation the overall peak temperatures were used to calculate the friction coefficient. Through this procedure a frictional coefficient of 0.15 to 0.2 was found to give comparable results to test data.

3.6 Parametric study Definitions for Butt and Lap welds

A parametric study was performed for FSW of butt and lap welds using the validated models. Parameters including tool travel rate, rotational tool speeds, and different workpiece materials were studied. These parameters dictate the overall workpiece temperature history, based on a literature review of many researchers [3, 10, 12, and 13] who studied them in their studies or analyses.

3.6.1 Butt Weld Model Correlation and Parametric Study Definitions

Model Verification for Butt Weld

In order to develop a useful thermal model for simulating FSW butt weld cases it was important to correlate the model to existing experimental data. Hence in this study the developed three-dimensional model has been correlated to the experimental data of Khandkar et al. [13].

The model used for correlation had sheet dimensions of 0.305 m by 0.105 m by 0.008 m of Al6061-T6 alloy material. The tool shoulder diameter was 0.025 m and tool pin diameter was 0.01 m. The tool pin length was 0.008 m and tool rpm was 390 rpm while the applied downward force on tool was taken to be 22.4 KN and tool travel rate was 140 mm/min.

Experimental measurements were made by Khandkar [14] through the use of twenty-five thermocouples embedded at different locations and depths in 3 layers in plate. These thermocouples were glued in the holes in plate by high temperature epoxy. Temperatures were recorded only on one side of the weldline as the overall process was symmetric about the weld centerline.

The graph in Figure 3.11, 3.12, and 3.13 show the comparison between instantaneous experimental and simulation results for top surface, mid surface, and bottom surface respectively. The workpiece temperatures were measured and calculated perpendicular to the weld line at $t = 75$ seconds i.e., at a distance of 190 mm from the end of the sheet. In Figure 3.11 the maximum top surface experimental temperature of 430°C was matched equally to the modeled temperature. The peak temperature at the edge of sheet was 75°C which matched the modeled temperature at that point. The overall trend was similar in both experimental and numerical case which is required for a good correlation. Some difference in between experimental and numerical temperature was seen ranging from $15\text{-}50^{\circ}\text{C}$ at 15mm to 30 mm from weld centerline. However difference could have been reduced if the installed operative error range of the thermocouples were known. A similar trend was seen for mid and bottom surface temperature profiles shown in Figure 3.12 and Figure 3.13.

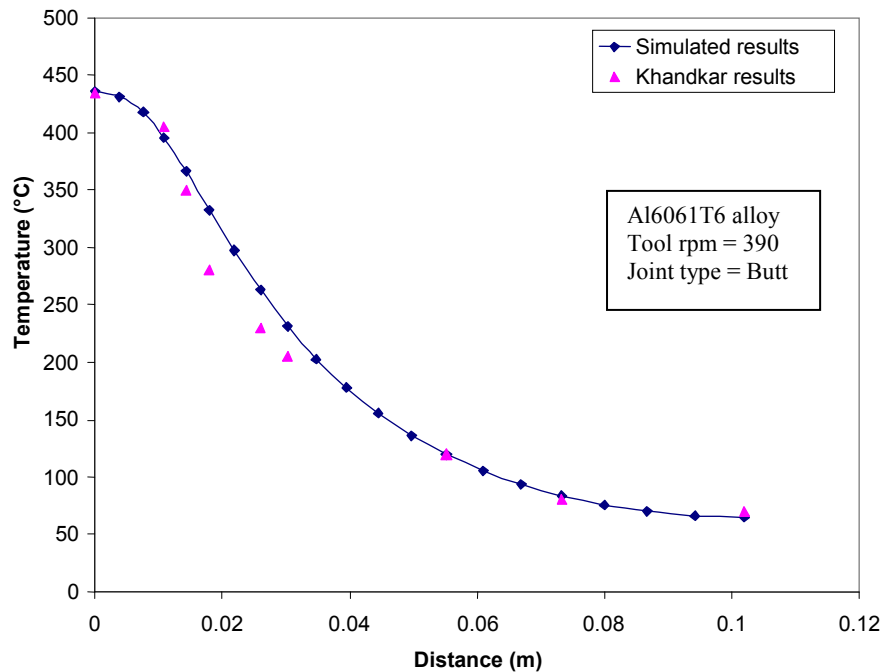


Figure 3.11. Comparison of simulated and experimental results recorded perpendicular to weld line on top surface for Al6061T6 at a distance of 190 mm from edge of sheet.

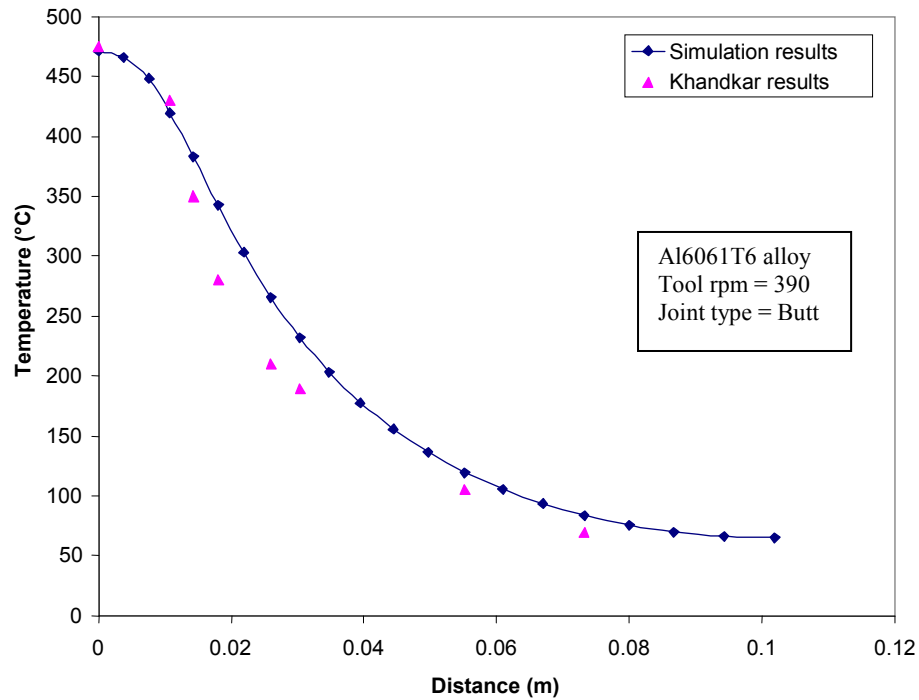


Figure 3.12 Comparison of simulated and experimental results recorded perpendicular to weld line on mid surface for Al6061T6 at a distance of 190 mm from edge of sheet.

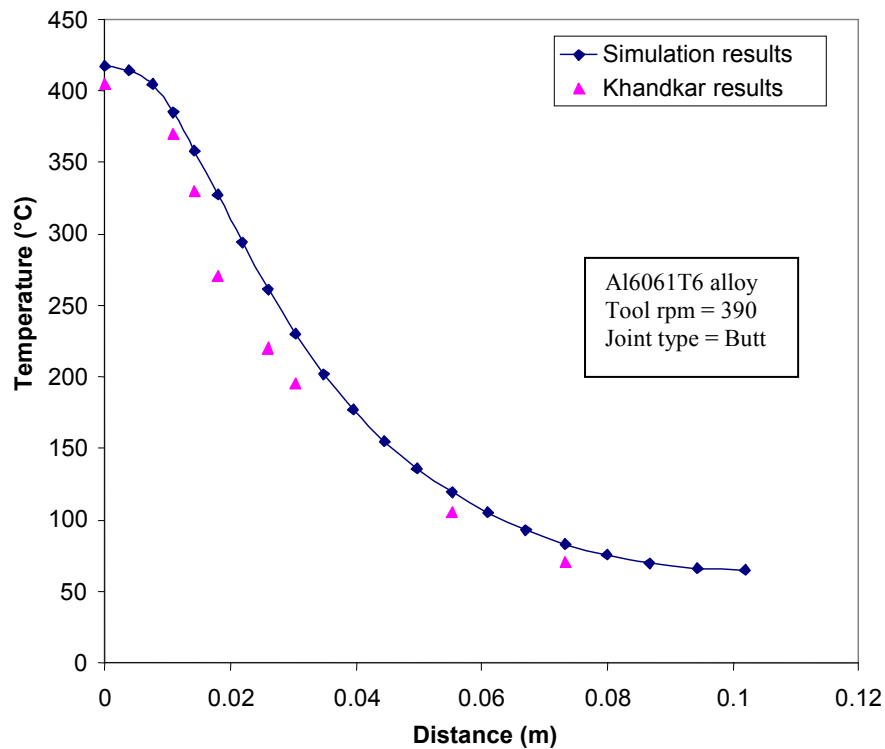


Figure 3.13. Comparison of simulated and experimental results recorded perpendicular to weld line on bottom surface for Al6061T6 at a distance of 190 mm from edge of sheet.

Parametric Study Definitions for Butt Weld

The results obtained from the simulations in Figure 3.11 to 3.13 correlated fairly well with the experimental top, mid and bottom surface temperature distributions. This correlated model for the butt weld was used for the subsequent parametric study, which included maintaining constant rotational speed, force on the tool, tool dimensions and the friction coefficient while varying the tool travel rate. Table 3.5 shows the summarized model descriptions for each of the cases considered.

Table 3.5

Model descriptions for various cases in the parametric study of a butt weld

	Case 1					Case 2				Case 3			
Alloy material	Al6061-T6					Al5052-H32				Al7050-T7451			
Sheet length (m)	0.305					0.305				0.305			
Sheet width (m)	0.102					0.102				0.105			
Sheet thickness (m)	0.00813					0.00813				0.00813			
Shoulder diameter (m)	0.025					0.025				0.025			
Pin diameter (m)	0.01					0.01				0.01			
Pin length (m)	0.008					0.008				0.008			
Travel rate (mm/min)	90	115	140	170	200	115	140	175	200	140	170	200	225
Rotational velocity (rad/s)	41 (390 rpm)					41 (390 rpm)				41 (390 rpm)			
Down tool force (KN)	22.4					22.4				22.4			
Bottom convection coefficient(W/m ² °C)	300					300				300			
Initial workpiece and ambient temperature (°C)	22					22				22			

Three travel rate cases have been studied involving 3 different aluminium alloys. The tool travel rate was chosen in accordance with the solidus temperature of different alloy types used such that the resultant temperature was below the solidus temperature of the alloy.

3.6.2 Lap Weld Model Correlation and Parametric Study Definitions

Model Verification for Lap Weld

In order to develop a useful model for obtaining the thermal history in the workpiece during the FSW of lap weld it is important to correlate the model to experimental data. Similarly to butt weld modeling, the goal was to match the maximum experimental temperature data of the workpiece with the simulated data. Hence in this study the developed three-dimensional model has been correlated to the experimental data published by Khandkar et al [14]. Table 3.6 shows the various correlation cases considered. Through a similar approach adopted as in the butt weld model, different combinations of friction coefficient and the bottom convective coefficient were used to correlate model temperature history to test data.

Best comparison between results at weldline were obtained for $\mu = 0.15$ and $h = 150 \text{ W/m}^2 \text{ }^\circ\text{C}$. Also these factors were in the range of the values that were used by various researchers [3, 8, 13,14] Once these two factors were calculated, the model was refined to get a good match between results obtained across the surface perpendicular to the weld-line through correlation cases 1 to 4. In cases 2 to 4 the thermal contact conductance was reduced by a factor of 10, 1000 and 100 respectively to check for possible effects of any contact resistance in between the faying surfaces of the two sheets as previously performed by Khandkar [14]. The differences in modeling approaches were the method of application of TCC at the contact surface and the equation used to calculate the basic thermal contact conductance (developed by

Madhusudana [25] as discussed in previous section). As the contact conditions between the sheets were not known and quantified this assumption was used to estimate the TCC.

Table 3.6

Correlation models for FSW of a lap weld

	Case 1	Case 2	Case 3	Case 4
Alloy material	Al5454-O	Al5454-O	Al5454-O	Al5454-O
Sheet length (m)	0.305	0.305	0.305	0.305
Sheet width (m)	0.102	0.102	0.102	0.102
Sheet thickness (m)	0.0018	0.0018	0.0018	0.0018
Shoulder diameter (m)	0.025	0.025	0.025	0.025
Pin diameter (m)	0.01	0.01	0.01	0.01
Pin length (m)	0.0028	0.0028	0.0028	0.0028
Variable Thermal Contact Conductance ($\text{W/m}^2 \text{ } ^\circ\text{C}$)	2.0E6 (fixed)	2.0E6*	2.0E6**	2.0E6***
Travel rate (mm/min)	140	140	140	140
Rotational velocity (rad/s)	52.33 (500 rpm)	52.33 (500 rpm)	52.33 (500 rpm)	52.33 (500 rpm)
Down tool force (KN)	17.5	17.5	17.5	17.5
Bottom convection coefficient ($\text{W/m}^2 \text{ } ^\circ\text{C}$)	150	150	150	150

* Thermal contact conductance between sheets decreased by 10 times beyond tool shoulder.

** Thermal contact conductance between sheets decreased by 100 times beyond tool shoulder.

*** Thermal contact conductance between sheets decreased by 1000 times beyond tool shoulder.

Figure 3.14 shows the correlation between the results from case 2, case 3 with the best fit (0% error line) curve. In this plot the results from either sides of weld centerline are taken and plotted against the 0% error line which is the perfect match case with experimental results being exactly

equal to simulation results. It is seen through the linear trendlines for both the cases that results from case 2 best match up to the perfect correlation scenario. Figure 3.15 shows the distribution of corresponding test and simulation results.

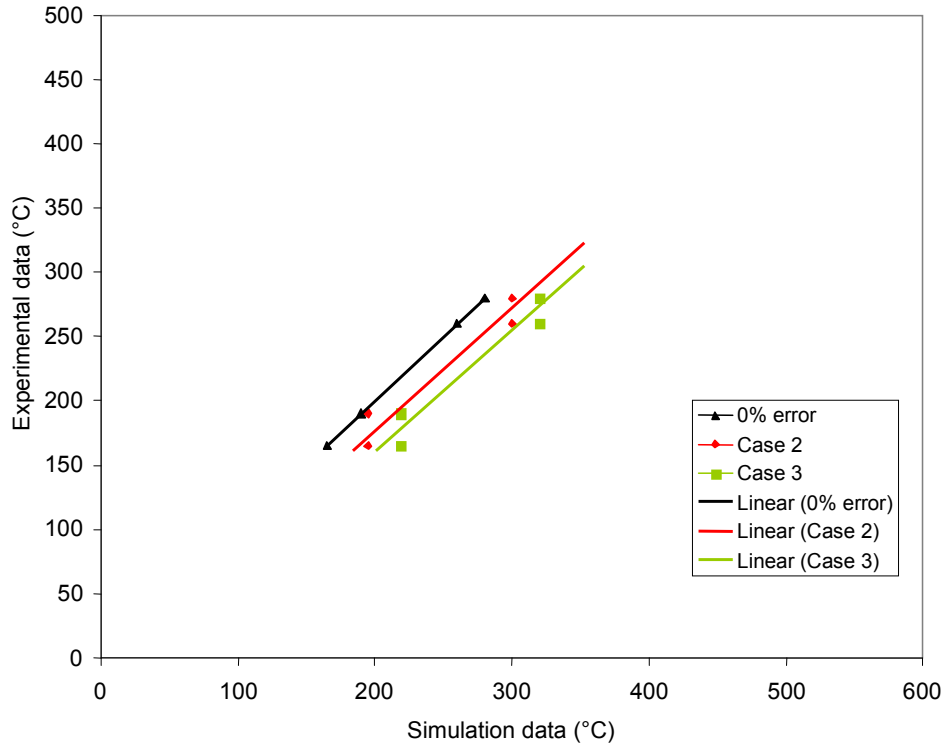


Figure 3.14. Correlation of case 2 and case 3 of lap weld with best fit (0% error) line.

Results from case 1 and case 4 produced inconclusive results in terms of the peak temperatures (510°C) and the minimum temperatures (190°C) obtained in the sheets which varied by 10 % from the experimental results. Hence were not included in the correlation chart. The successful correlation case 2 model was taken for further parametric studies and analyses. Figure 3.15 and 3.16 show the comparison of results for top surface and mid surface respectively from the case 2 model. As seen from Figure 3.13 three data points out of four data points match to a great extent with the maximum difference being less than 10°C. The extent of correlation between experimental and calculated workpiece temperature could have more precisely defined if the installed operative error range of the thermocouples used in the experiments were known.

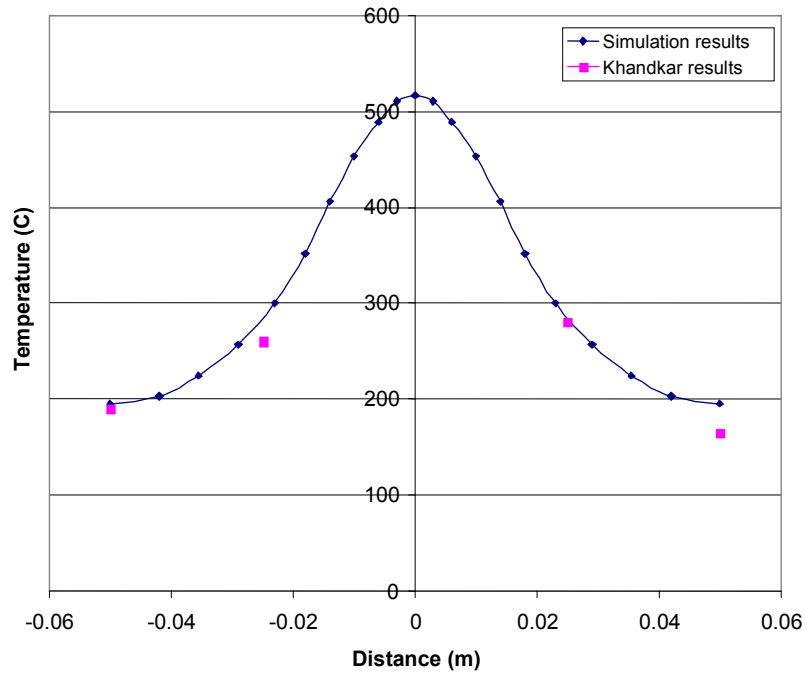


Figure 3.15. Comparison of simulated and experimental results recorded for lap weld perpendicular to weld line on top surface at a distance of 190 mm from the edge of sheet.

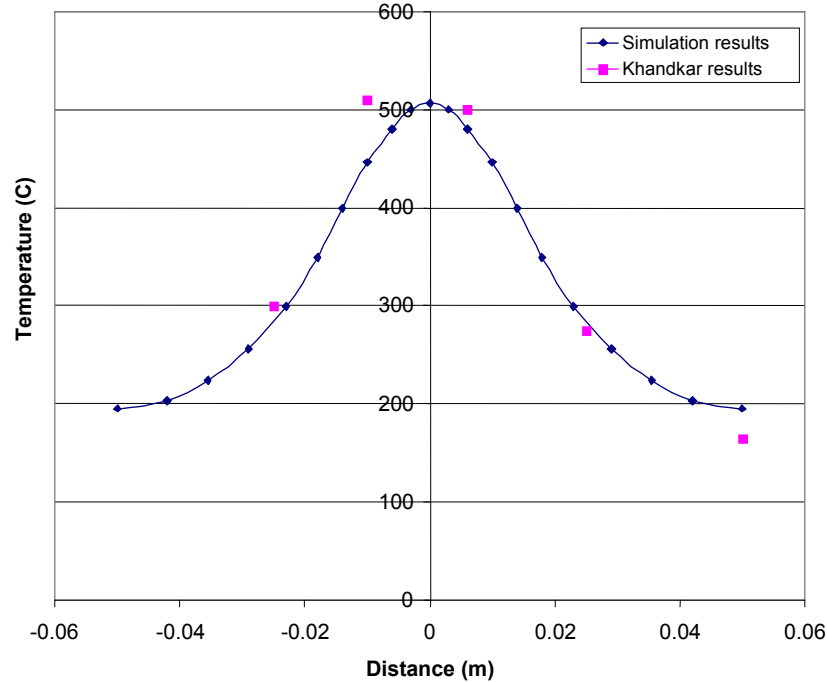


Figure 3.16. Comparison of simulated and experimental results recorded for lap weld perpendicular to weld line on mid surface at a distance of 190 mm from the edge of sheet.

Parametric Study Definitions for Lap Weld

In this study the parameters included force on the tool, tool dimensions and the friction coefficient, all of which were kept constant. Table 3.7 shows the summarized model descriptions for the first three cases considered. Table 3.8 shows the details for case 4.

Table 3.7

Model descriptions for various cases in the parametric study of lap welds

	Case 1			Case 2			Case 3		
Alloy material	Al2024-T3			Al6061-T6			Al7050-T7451		
Sheet length (m)	0.305			0.305			0.305		
Sheet width (m)	0.102			0.102			0.102		
Sheet thickness (m)	0.0018			0.0018			0.0018		
Shoulder diameter (m)	0.025			0.025			0.025		
Pin diameter (m)	0.01			0.01			0.01		
Pin length (m)	0.0028			0.0028			0.0028		
Travel rate (mm/min)	140	180	220	100	140	180	100	125	150
Rotational velocity (rad/s)	52.33 (500 rpm)			52.33 (500 rpm)			52.33 (500 rpm)		
Down tool force (KN)	17.5			17.5			17.5		
Bottom convection coefficient ($W/m^2 \text{ } ^\circ C$)	150			150			150		
Initial process temperature ($^\circ C$)	25			25			25		

The parameter varied here was the tool travel rate in cases 1 to 3 while in case 4 the tool travel rate was kept constant and the rotational speed was varied to observe the peak temperatures obtained through the top, mid and bottom surfaces. The parameters were chosen such that the

resultant peak temperatures were below the solidus temperature of each alloy used in the analyses. These parameters were within commonly used parameters in current research [3, 10, and 14].

Table 3.8

Model description for case 4 of lap weld in the parametric study

	Case 4		
Alloy material	Al2024-T3		
Sheet length (m)	0.305		
Sheet width (m)	0.102		
Sheet thickness (m)	0.0018		
Shoulder diameter (m)	0.025		
Pin diameter (m)	0.01		
Pin length (m)	0.0028		
Travel rate (mm/min)	140	180	220
Tool rotational velocity (rad/s)	41.86 (400 rpm)	41.86 (400 rpm)	41.86 (400 rpm)
	52.33 (500 rpm)	52.33 (500 rpm)	52.33 (500 rpm)
	62.8 (600 rpm)	62.8 (600 rpm)	62.8 (600 rpm)
Down tool force (KN)	17.5		
Bottom convection coefficient ($\text{W/m}^2 \text{ } ^\circ\text{C}$)	150		
Initial workpiece and ambient temperature ($^\circ\text{C}$)	25		

CHAPTER 4

RESULTS AND DISCUSSIONS

4.1 Butt Weld Simulation Results

Three cases for parametric study were considered with Case 1 for Al6061T6 with tool travel rates varied from 90 mm/min to 200 mm/min, Case 2 for Al5052H32 alloy with tool travel rates varied from 115 mm/min to 200 mm/min and Case 3 for Al7050 alloy with travel rates varied from 140 to 200 mm/min. The tool travel rates were chosen such that the obtained workpiece temperatures were below the solidus temperature required for good FSW butt weld.

4.1.1 Case 1: Al6061-T6 alloy

Figures 4.1.1, 4.1.2, and 4.1.3 show the temperature contours obtained at 2 seconds, 60 seconds and 107 seconds respectively for a tool travel rate of 90 mm/min. Figure 4.1.4 shows the temperature contours through the weld seam obtained at 60 seconds.

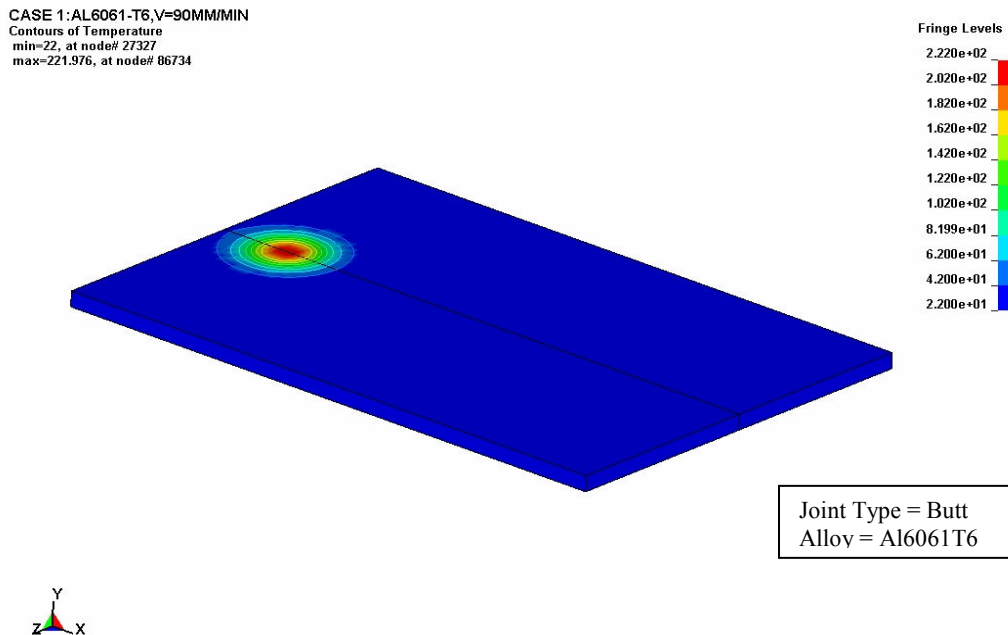
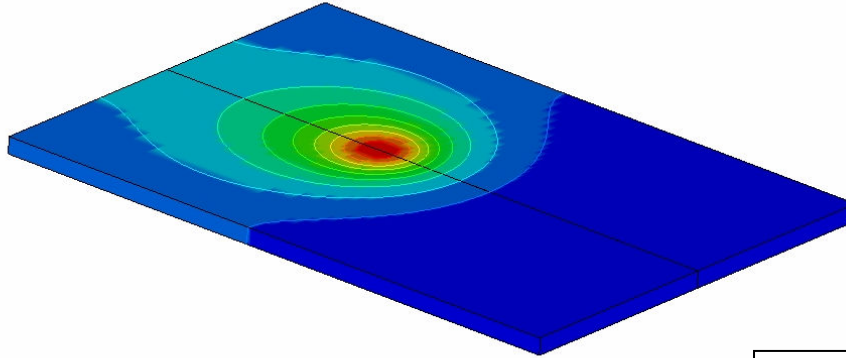


Figure 4.1.1. Top surface temperature contours after 2 sec at tool travel rate of 90 mm/min.

CASE 1:AL6061-T6,V=90MM/MIN
Contours of Temperature
min=22.4939, at node# 25270
max=501.337, at node# 43184

Fringe Levels
5.013e+02
4.535e+02
4.056e+02
3.577e+02
3.098e+02
2.619e+02
2.140e+02
1.661e+02
1.183e+02
7.038e+01
2.249e+01



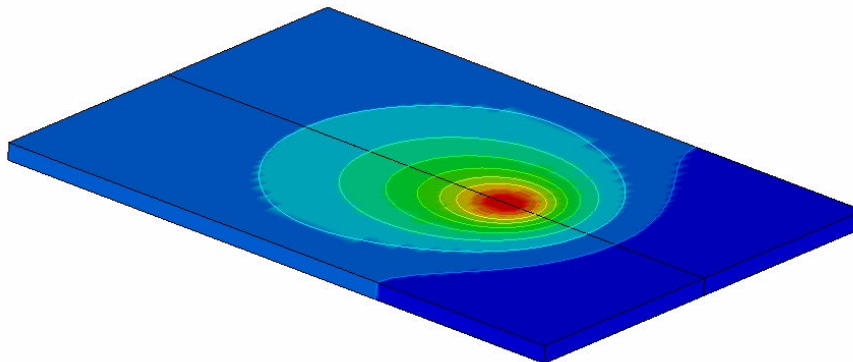
Joint Type = Butt
Alloy = Al6061T6



Figure 4.1.2. Top surface temperature contours after 60 sec at tool travel rate of 90 mm/min.

CASE 1:AL6061-T6,V=90MM/MIN
Contours of Temperature
min=34.1981, at node# 25270
max=512.245, at node# 89422

Fringe Levels
5.122e+02
4.644e+02
4.166e+02
3.688e+02
3.210e+02
2.732e+02
2.254e+02
1.776e+02
1.298e+02
8.200e+01
3.420e+01



Joint Type = Butt
Alloy = Al6061T6



Figure 4.1.3. Top surface temperature contours after 107 sec at tool travel rate of 90 mm/min.

CASE 1:AL6061-T6,V=90MM/MIN
Contours of Temperature
min=25.8473, at node# 70250
max=509.264, at node# 88876

Joint Type = Butt
Alloy = Al6061T6

Fringe Levels

5.093e+02
4.609e+02
4.126e+02
3.642e+02
3.159e+02
2.676e+02
2.192e+02
1.709e+02
1.225e+02
7.419e+01
2.585e+01



Figure 4.1.4. Temperature contours through the weld seam at a tool travel rate of 90 mm/min.

Figure 4.1.5, 4.1.6, and 4.1.7 show the instantaneous temperature profiles for linear tool velocities of 90 mm/min, 115 mm/min, and 140 mm/min respectively at a distance of 190 mm from the initial position of start of weld. Figure 4.1.7 shows the variation of temperature on top surface for different tool travel rates.

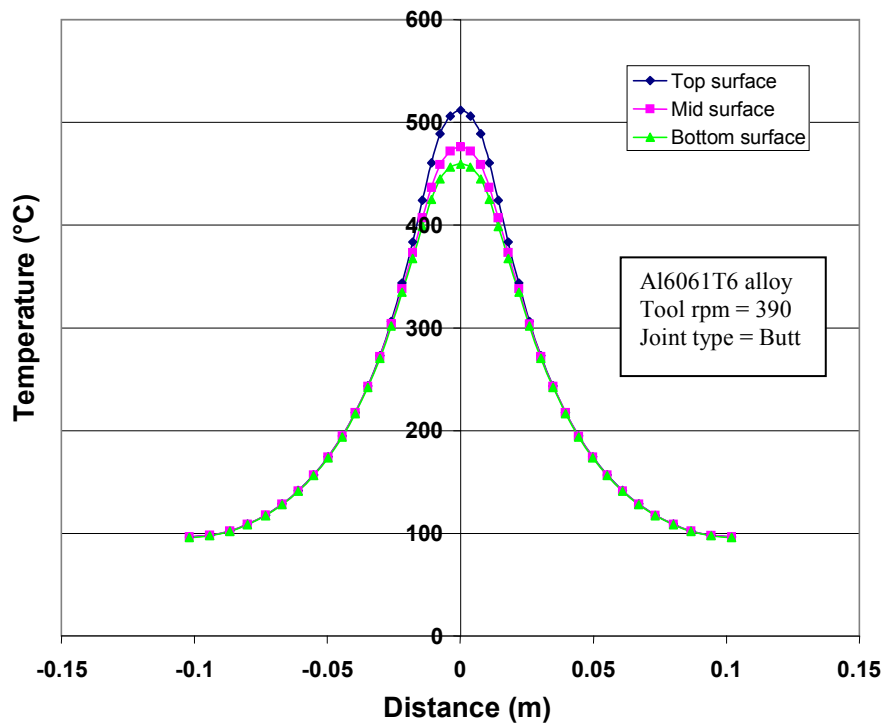


Figure 4.1.5. Instantaneous temperature profiles perpendicular to weld line at 90 mm/min.

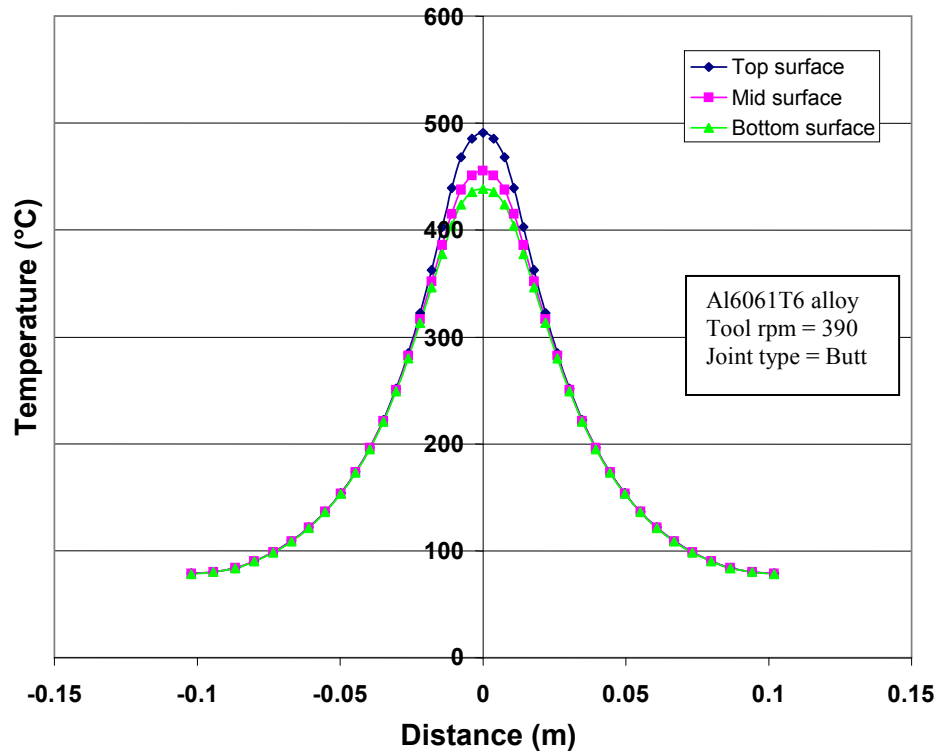


Figure 4.1.6. Instantaneous temperature profiles perpendicular to weld line at 115 mm/min.

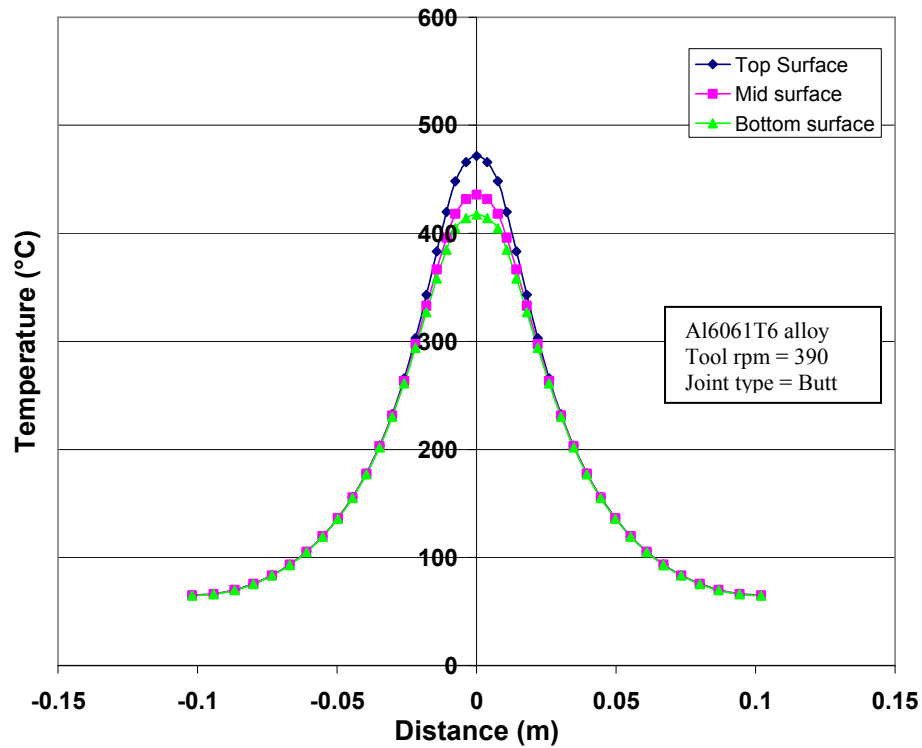


Figure 4.1.7. Instantaneous temperature profiles perpendicular to weld line at 140 mm/min.

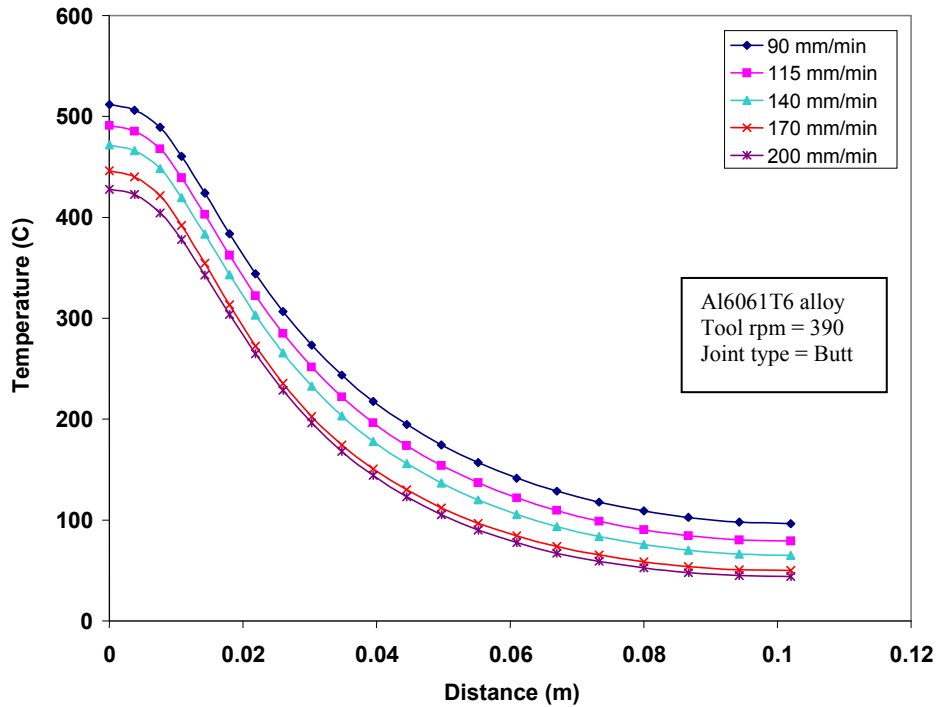


Figure 4.1.8. Variation of temperature on top surface for different tool travel rates.

Temperature contour plots from Figure 4.1.1 to 4.1.3 show thermal profiles similar to that seen in FSW applications, similarly the contour plots show constant heating effect taking place ahead of the tool which is typical for a FSW process. A linear relationship was observed between the travel rate and peak temperature.

It is also seen from the temperature history plots from Figure 4.1.8 for Al6061-T6 alloy that the maximum or peak temperature obtained varied between 510°C and 430°C for tool travel rates varying from 90 mm/min to 200 mm/min for a constant tool rpm of 390 rpm. As expected the slower the travel rate, the higher the temperature as there is more time for localized workpiece heating. Also the minimum temperature obtained varied between 97°C to 45°C at the edge of sheet perpendicular to weld line. Good weld quality could be obtained for peak temperatures in between 450°C to 510°C [3] which is possible with welding speeds in the range of 90 mm/min to 170 mm/min for a tool rpm of 390 rpm. For all tool travel rates a constant

temperature difference between top surface to mid surface and mid surface to bottom surface was seen. Possibly due to the high thermal conductivity of material compared to heat accumulation from thermal capacitance. This difference was 35°C in between the top surface and mid surface while 17°C was the difference between the mid surface and bottom surface temperature.

4.1.2 Case 2: Al 5052-H32 alloy

Figure 4.2.1, 4.2.2, and 4.2.3 show the instantaneous temperature profiles for linear tool velocities of 115 mm/min, 140 mm/min, and 175 mm/min respectively at a distance of 190 mm from the edge of the Al5052-H32 sheet. Figure 4.2.4 shows the variation of temperature on top surface for different tool travel rates. The temperatures were recorded after a process time of 92 seconds, 76 seconds, 62 seconds and 54 seconds for linear speeds of 115 mm/min, 140 mm/min, 175 mm/min, and 200 mm/min respectively. The process time for travel rates of 115 mm/min, 140 mm/min, and 175 mm/min was 115 seconds, 95 seconds, and 77 seconds respectively.

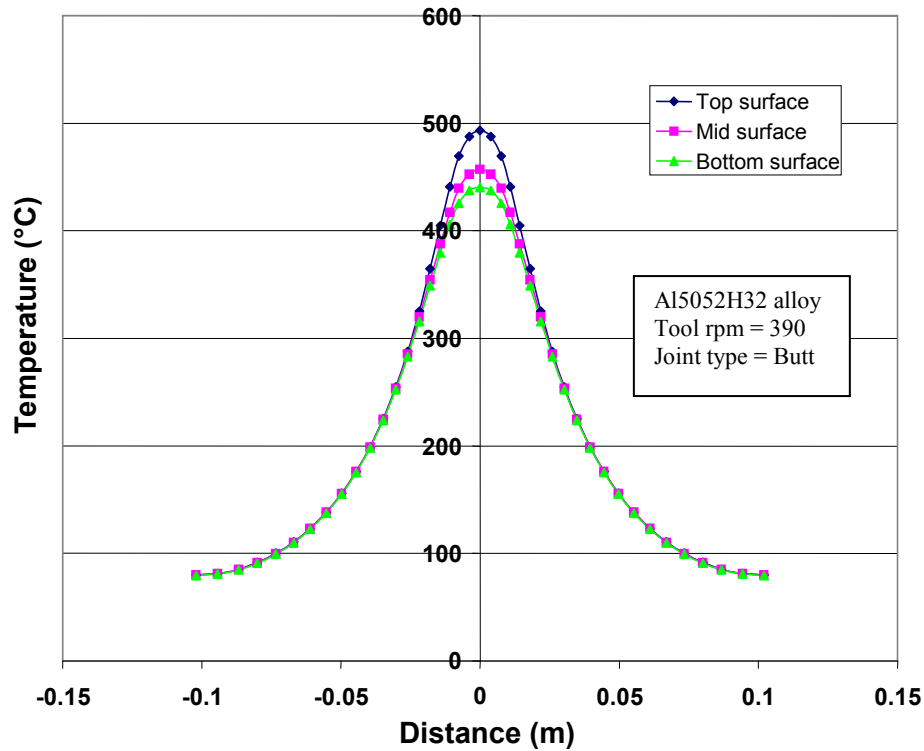


Figure 4.2.1. Instantaneous temperature profiles perpendicular to weld line at 115 mm/min.

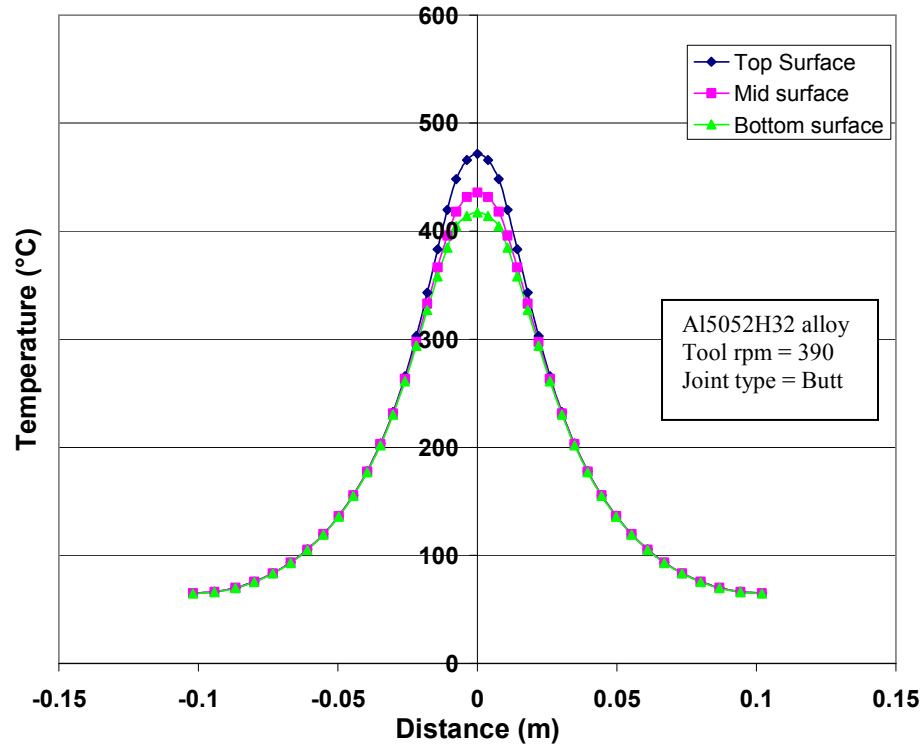


Figure 4.2.2. Instantaneous temperature profiles perpendicular to weld line at 140 mm/min.

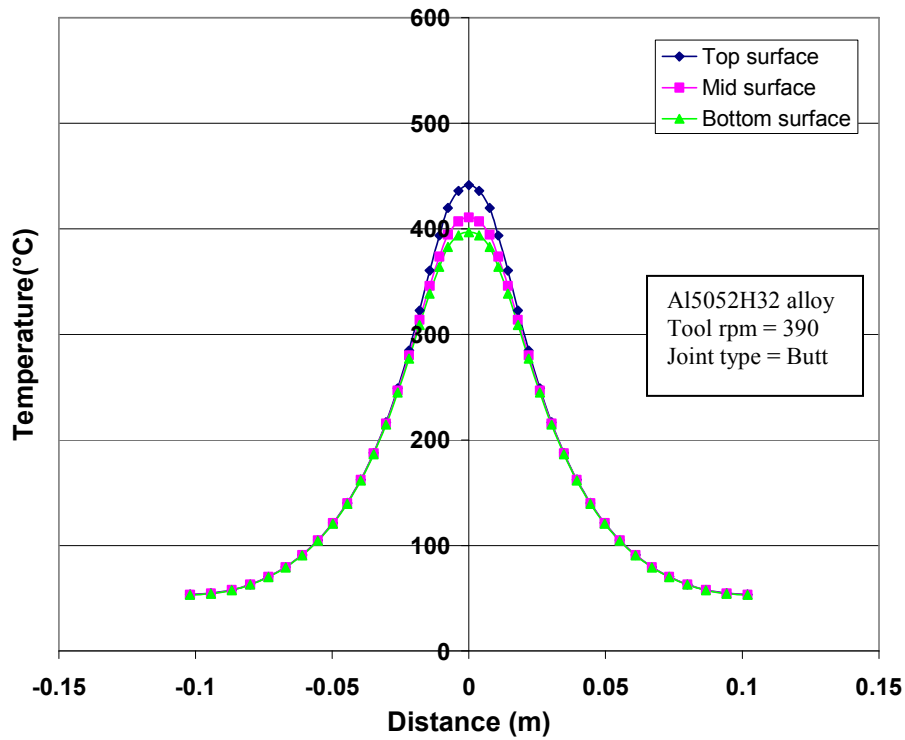


Figure 4.2.3. Instantaneous temperature profiles perpendicular to weld line at 175 mm/min.

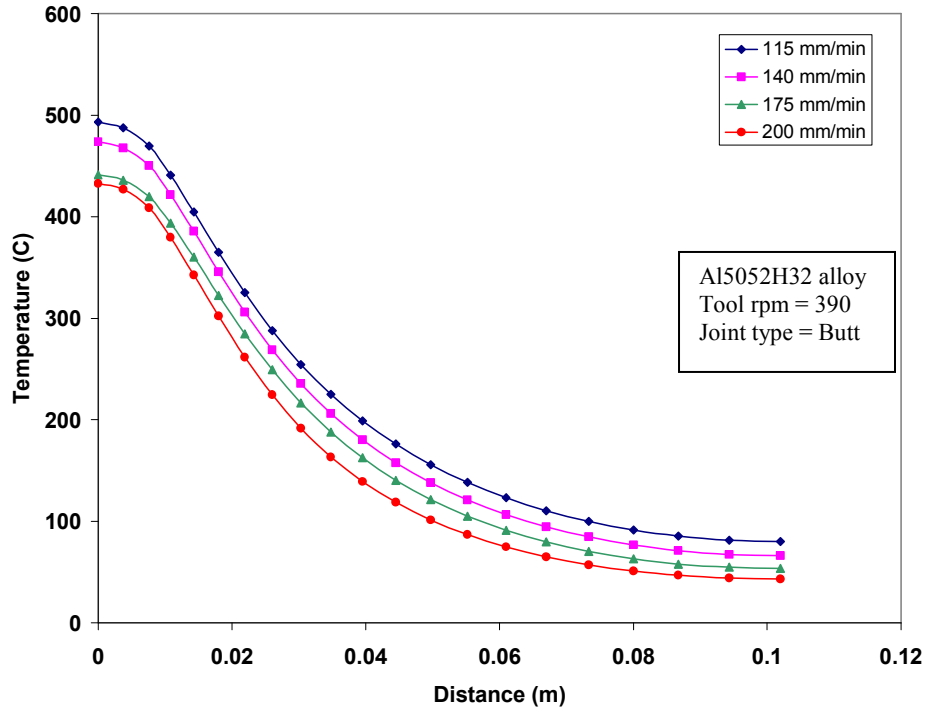


Figure 4.2.4. Variation of temperature on top surface for different tool travel rates.

It is seen from the temperature history plot from Figure 4.2.4 for Al5052-H32 alloy that the maximum or peak temperature obtained varies in between 495°C and 432°C for tool travel rate varying from 115 mm/min to 200 mm/min at constant tool rpm of 390 rpm. Also the minimum temperature obtained varied in between 80°C to 43°C at edge sheet perpendicular to weld line. Good weld quality could be obtained for peak temperatures in between 450°C to 510°C which is possible with welding speeds in the range of 115 mm/min to 175 mm/min for a tool rpm of 390 rpm. Similar to the previous case, for the travel rates considered a constant difference in temperature between top surface to mid surface and mid surface to bottom surface was seen possibly due to the high thermal conductivity of the material compared to the heat accumulation from thermal capacitance. This difference was 37°C in between the top surface and mid surface while 17°C was the difference between the mid surface and bottom surface temperature.

4.1.3 Case 3: Al7050-T7451

Figure 4.3.1, 4.3.2, and 4.3.3 show the instantaneous temperature profiles for tool travel rates of 140 mm/min, 170 mm/min, and 200 mm/min respectively at a distance of 190 mm from the starting location of the tool on the Al7050-T7451 sheet. Figure 4.3.4 shows the variation of temperature on top surface for different tool travel rates. The temperature were recorded after a process time of 75 seconds, 63 seconds, 54 seconds, and 48 seconds for linear speeds of 140 mm/min, 170 mm/min, 200 mm/min, and 225 mm/min respectively. The computation time for linear speeds of 140 mm/min, 170 mm/min, and 200 mm/min was 95 seconds, 79 seconds, and 67 seconds respectively. From the heat source reference, the temperature distribution at each instant is a quasi-steady state mode. It was seen through these plots that the shape profiles for different travel rates were similar with difference being in the peak temperatures and having constant ΔT in between the surfaces.

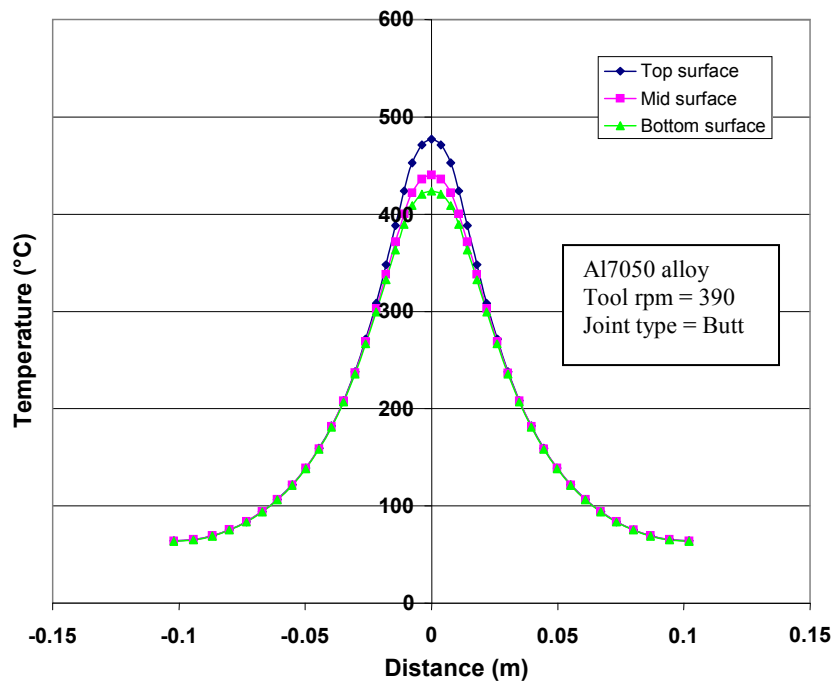


Figure 4.3.1. Instantaneous temperature profiles perpendicular to weld line at 140 mm/min.

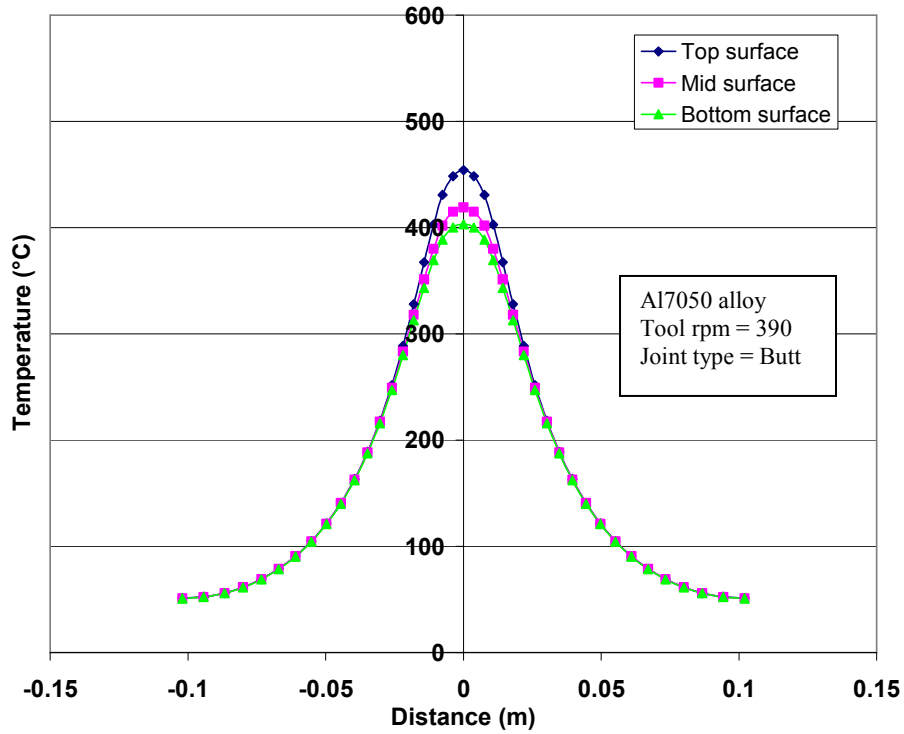


Figure 4.3.2. Instantaneous temperature profiles perpendicular to weld line at 170 mm/min.

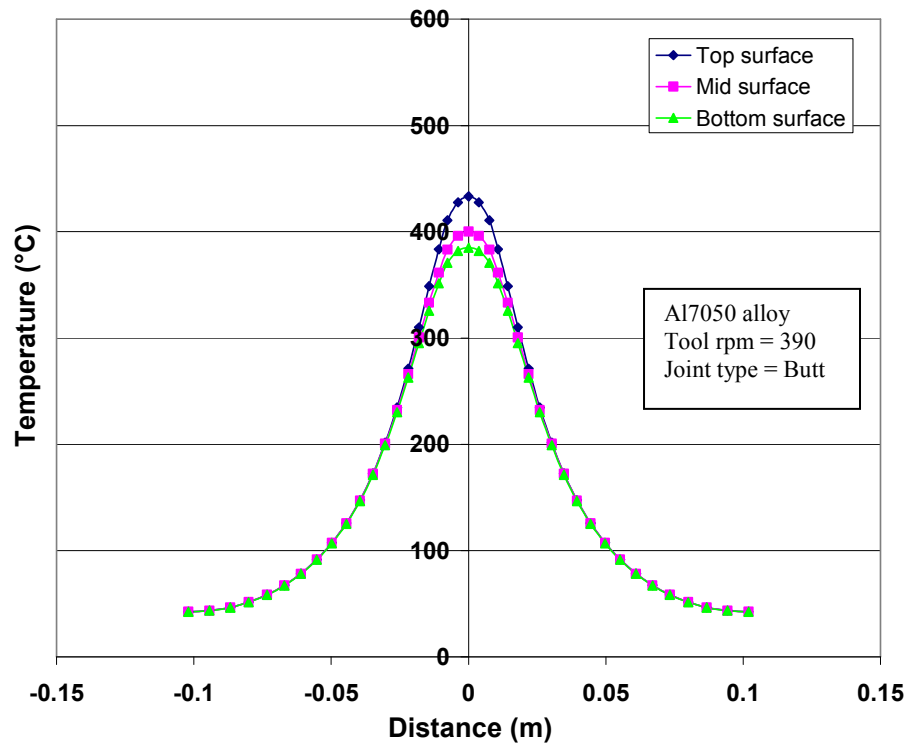


Figure 4.3.3. Instantaneous temperature profiles perpendicular to weld line at 200 mm/min.

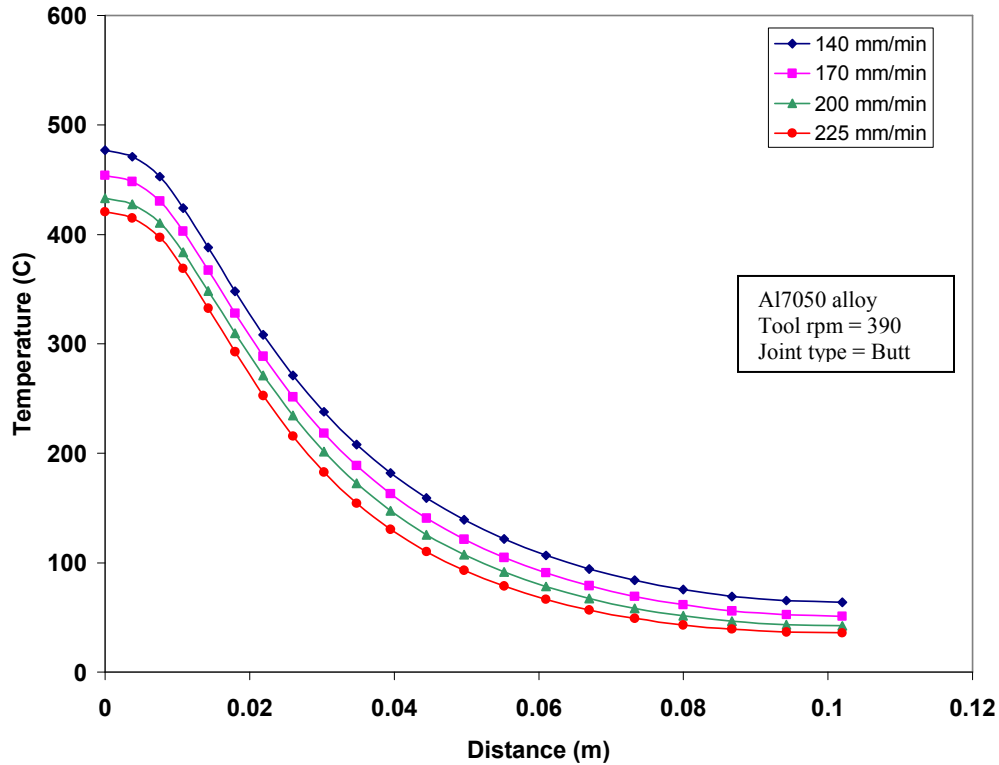


Figure 4.3.4. Variation of temperature on top surface for different tool travel rates.

It is seen from the temperature history plots from Figure 4.3.4 for Al7050-T7451 alloy that the maximum or peak temperature obtained varied in between 477°C and 422°C for tool travel rates varying from 140 mm/min to 225 mm/min at constant tool rpm of 390 rpm. Also the minimum temperature obtained at edge of sheet perpendicular to weld line varied in between 64°C to 36°C. Similar to previous cases, the slower the travel rate, the higher the temperature as there is more time for localized workpiece heating. Good weld quality could be obtained for peak temperatures in between 420°C to 490°C which is possible with welding speeds in the range of 140 mm/min to 225 mm/min for a tool rpm of 390 rpm. For all the linear speeds a constant difference in temperature between top surface to mid surface and mid surface to bottom surface was seen. This difference was 36°C in between the top surface and mid surface while 16°C was the difference between the mid surface and bottom surface temperature. Possibly due to the high thermal conductivity of material compared to heat accumulation from thermal capacitance.

Summary of Results for FSW of Butt Weld

Table 4.1, 4.2, and 4.3 show the tabulated peak temperature results for butt weld of Al6061-T6, Al5052-H32, and Al7050-T7451 respectively.

Table 4.1

Summary of peak temperatures for butt weld of Al6061-T6

Material	Tool rotational velocity (rpm)	Tool travel rate (mm/min)	Top surface peak temperature (°C)	Mid surface peak temperature (°C)	Bottom surface peak temperature (°C)
Al6061-T6	390	90	512	476	459
		115	491	455	439
		140	472	436	417
		170	446	407	390
		200	428	395	380

Table 4.2

Summary of peak temperatures for butt weld of Al5052-H32

Material	Tool rotational velocity (rpm)	Tool travel rate (mm/min)	Top surface peak temperature (°C)	Mid surface peak temperature (°C)	Bottom surface peak temperature (°C)
Al6061-T6	390	115	493	457	440
		140	473	437	421
		175	441	411	397
		200	432	395	378

Table 4.3

Summary of peak temperatures for butt weld of Al7050-T7451

Material	Tool rotational velocity (rpm)	Tool travel rate (mm/min)	Top surface peak temperature (°C)	Mid surface peak temperature (°C)	Bottom surface peak temperature (°C)
Al7050-T7451	390	140	477	440	423
		170	454	419	403
		200	433	400	385
		225	421	384	368

4.2 Lap Weld Simulation Results

Four cases for parametric study were considered: Case 1 for Al2024T3 with tool travel rates varied from 140 mm/min to 220 mm/min, Case 2 for Al6061T6 alloy with tool travel rates varied from 100 mm/min to 180 mm/min, Case 3 for Al7050 alloy with travel rates 100 to 150 mm/min and Case 4 for Al2024T3 alloy with travel rates varied from 140 to 220 mm/min and rotational tool speeds varied from 400 to 600 rpm. The tool travel rates and rotational speeds were chosen such that the obtained workpiece temperatures were below the solidus temperature required for good FSW butt weld.

4.2.1 Case 1: Al2024-T3 alloy

Figures 4.4.1, 4.4.2, and 4.4.3 show the temperature contours obtained at 2 seconds, 38 seconds and 80 seconds respectively for a weld speed of 140 mm/min. this represents the weld start, halfway through the weld (pseudo-steady state) and near end of weld. Figure 4.4.4 shows the cross-sectional view of temperature contours through the weld seam at 38 seconds.

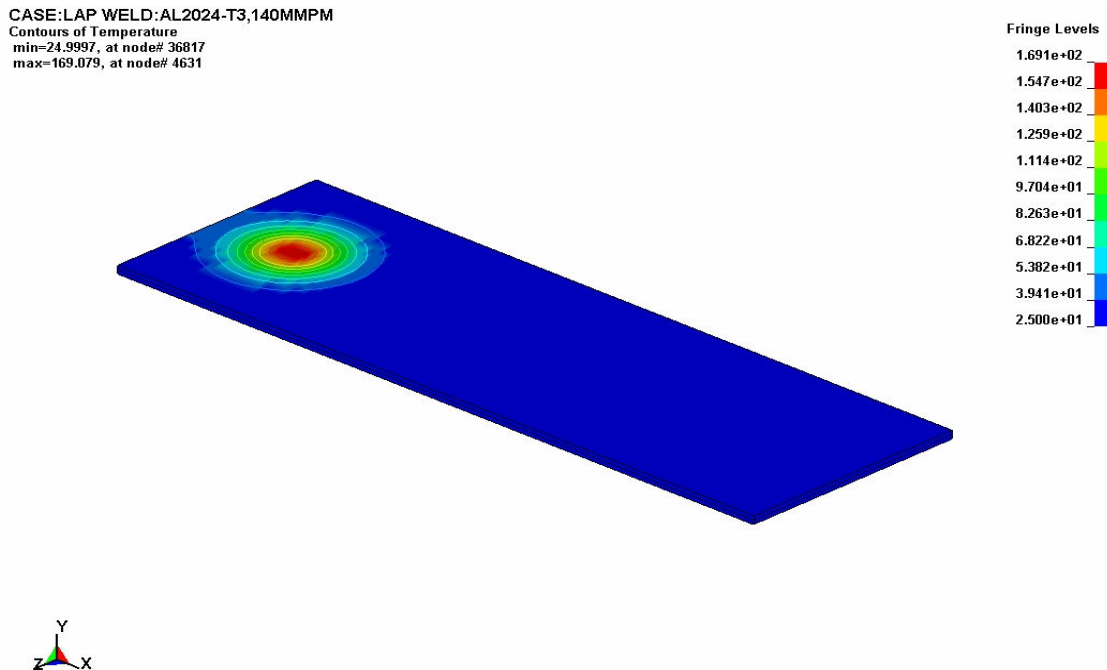


Figure 4.4.1 Top surface temperature contours after 2 sec at tool travel rate of 140 mm/min.

CASE:LAP WELD:AL2024-T3,140MMPM
 Contours of Temperature
 min=25.1854, at node# 50853
 max=422.658, at node# 3224

Fringe Levels
 4.227e+02
 3.829e+02
 3.432e+02
 3.034e+02
 2.637e+02
 2.239e+02
 1.842e+02
 1.444e+02
 1.047e+02
 6.493e+01
 2.519e+01

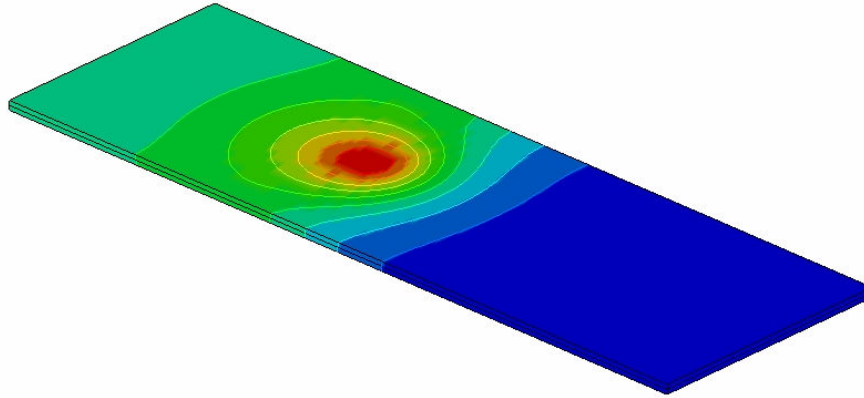


Figure 4.4.2. Top surface temperature contours after 38 sec at tool travel rate of 140 mm/min.

CASE:LAP WELD:AL2024-T3,140MMPM
 Contours of Temperature
 min=55.7656, at node# 50853
 max=448.622, at node# 1523

Fringe Levels
 4.486e+02
 4.093e+02
 3.701e+02
 3.308e+02
 2.915e+02
 2.522e+02
 2.129e+02
 1.736e+02
 1.343e+02
 9.505e+01
 5.577e+01

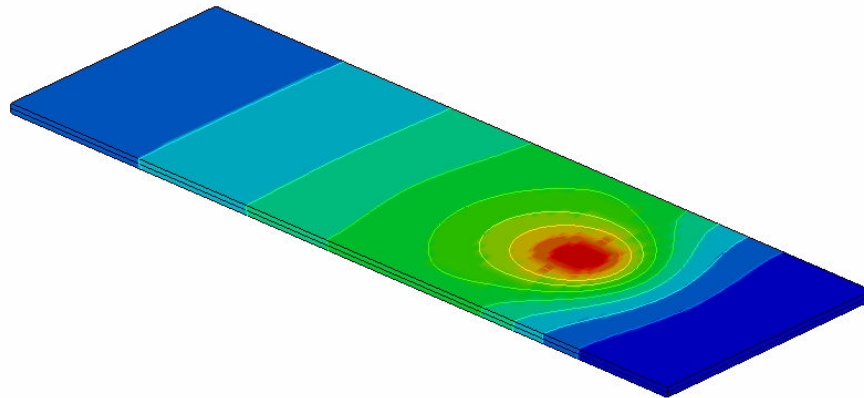


Figure 4.4.3. Top surface temperature contours after 80 sec at tool travel rate of 140 mm/min.

CASE:LAP WELD:AL2024-T3,140MMPM
 Contours of Temperature
 min=45.349, at node# 50853
 max=447.27, at node# 1712

Fringe Levels

4.473e+02
4.071e+02
3.669e+02
3.267e+02
2.865e+02
2.463e+02
2.061e+02
1.659e+02
1.257e+02
8.554e+01
4.535e+01



Figure 4.4.4. Cross-sectional view of temperature contours through the weld seam.

Figure 4.4.5, 4.4.6, and 4.4.7 show the instantaneous temperature profiles for linear tool velocities of 140 mm/min, 180 mm/min, and 220 mm/min respectively at a distance of 190 mm from the edge of the Al6061-T6 sheet. The temperatures were recorded after a process time of 82 seconds, 65 seconds, and 54 seconds for linear speeds of 140 mm/min, 180 mm/min, and 220 mm/min respectively. At this stage the heat transfer process is in a pseudo-steady state operation.

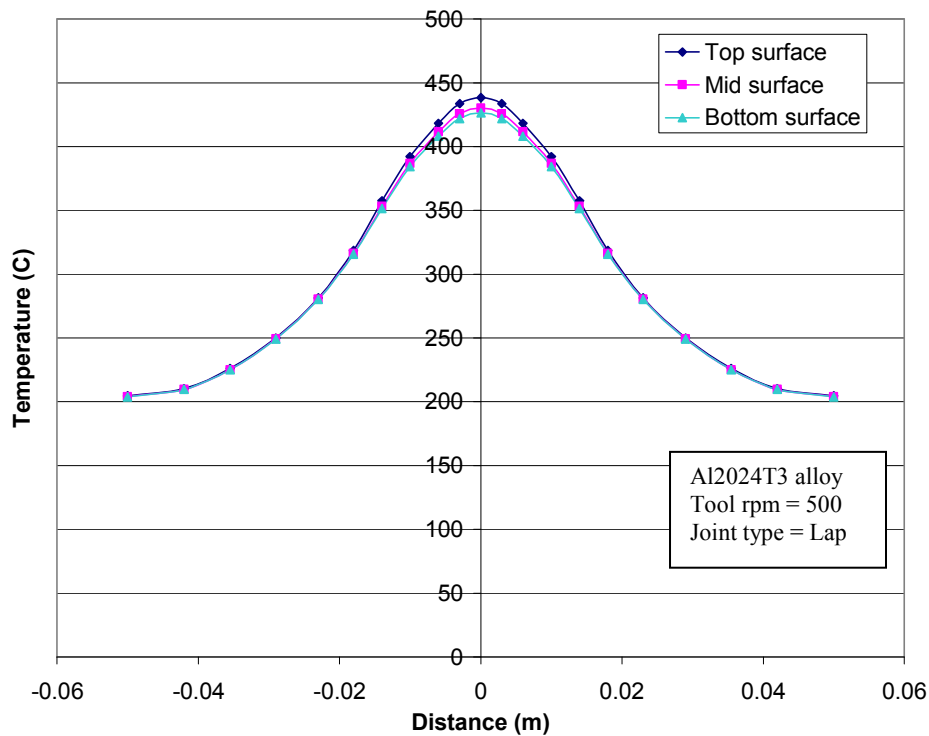


Figure 4.4.5. Instantaneous temperature profiles at perpendicular to weld line at 140 mm/min.

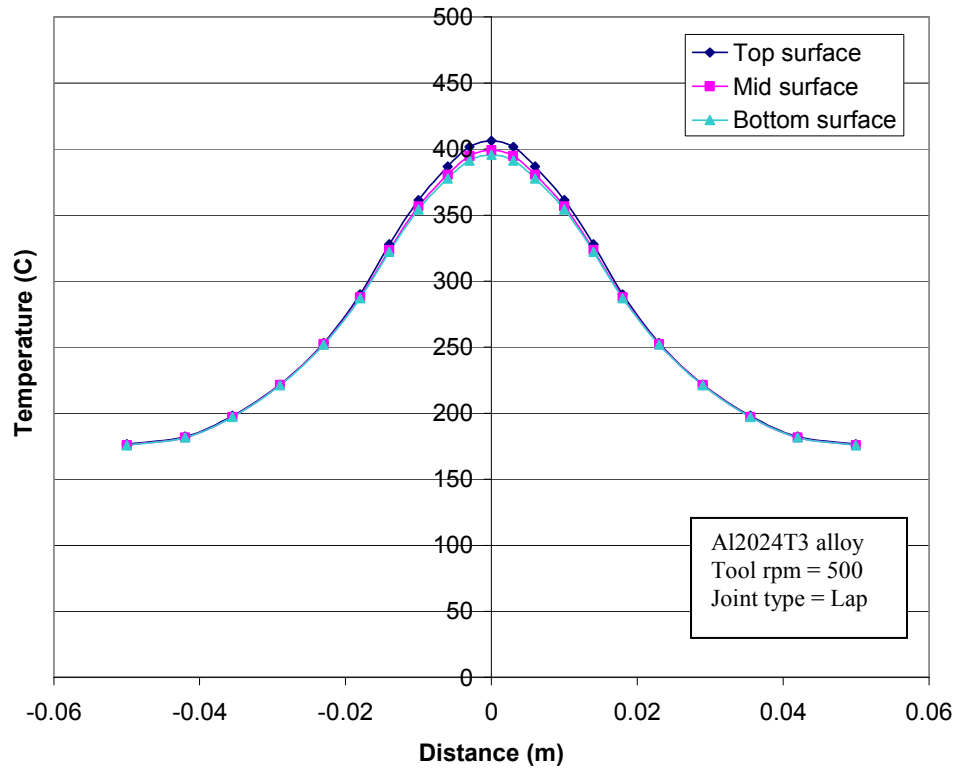


Figure 4.4.6. Instantaneous temperature profiles perpendicular to weld line at 180 mm/min.

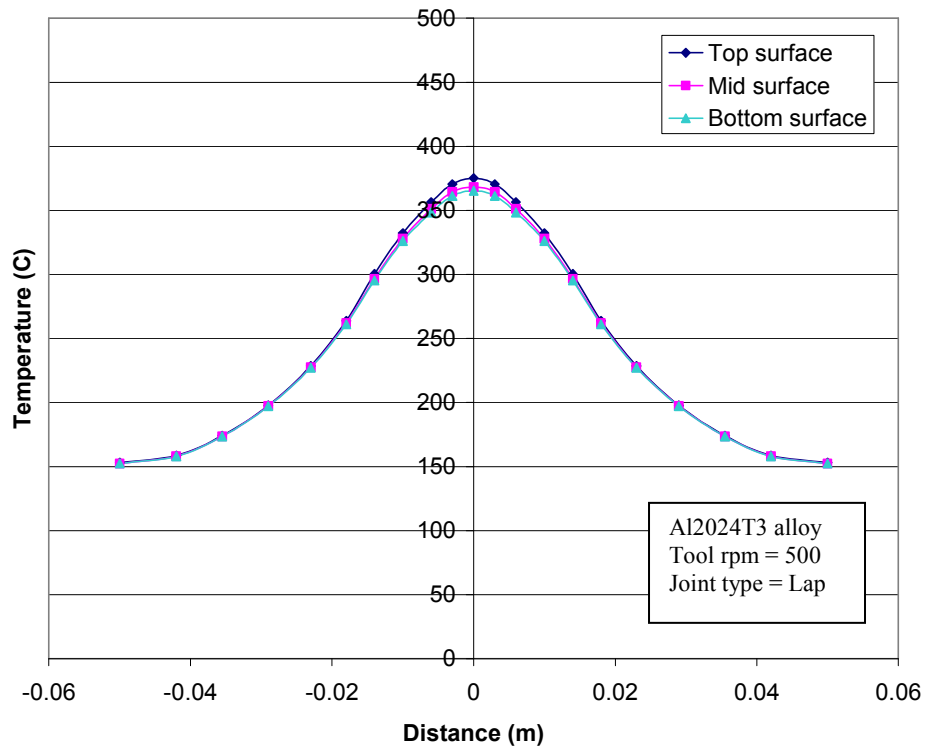


Figure 4.4.7. Instantaneous temperature profiles perpendicular to weld line at 220 mm/min.

It is seen from the temperature contours in Figures 4.4.1 to 4.4.3 that the peak temperature occurs mainly in the tool shoulder area and there is a constant heating taking place in region ahead of the tool similar to the actual lap weld process. Also the peak temperature across the thickness develops upto a depth of 2 mm which is mainly due to the tool pin that has penetrated the sheet surface upto a depth of 2.8 mm which is the pin length.

It is also seen from the temperature history plots for Al2024-T3 alloy that the maximum or peak temperature obtained varied in between 440°C and 375°C for tool travel rates varying from 140 mm/min to 220 mm/min at constant tool rpm of 500 rpm. Also the minimum temperature obtained varied in between 205°C to 153°C. As expected the slower the tool travel rate, higher the temperature obtained. Good weld quality could be obtained for peak temperatures in between 420°C to 490°C which is possible with welding speeds in the range of 140 mm/min to 180 mm/min for a tool rpm of 500 rpm. For all the linear speeds a constant difference in temperature between top surface to mid surface and mid surface to bottom surface was seen. Possibly due to high thermal conductivity of the workpiece compared to heat accumulation from thermal capacitance. This difference was 8°C in between the top surface and mid surface while 4°C was difference between the mid surface and bottom surface temperature.

4.2.2 Case 2: Al6061-T6 alloy

Figures 4.5.1, 4.5.2, and 4.5.3 show the instantaneous temperature profiles for tool travel rates of 100 mm/min, 140 mm/min, and 180 mm/min respectively at a distance of 190 mm from the start location of tool on Al6061-T6 sheet. The temperatures were recorded after a process time of 15 seconds, 82 seconds, and 65 seconds for tool travel rates of 100 mm/min, 140 mm/min, and 80 mm/min respectively. From the reference frame of heat source, the temperature distribution at an instant resulted from a quasi-steady state heat transfer mode.

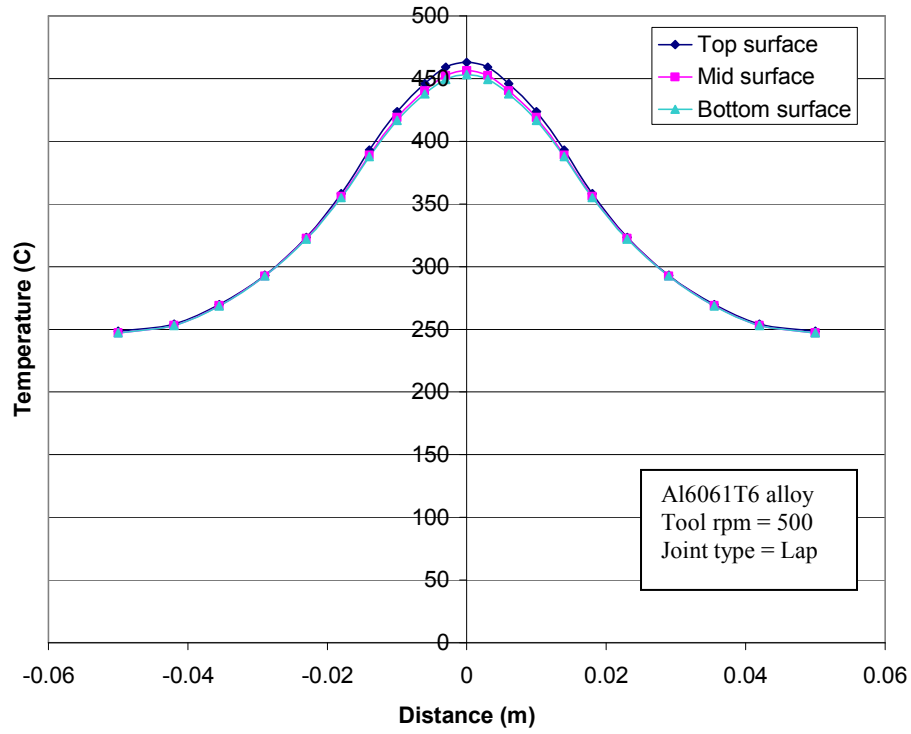


Figure 4.5.1. Instantaneous temperature profiles perpendicular to weld line at 100 mm/min.

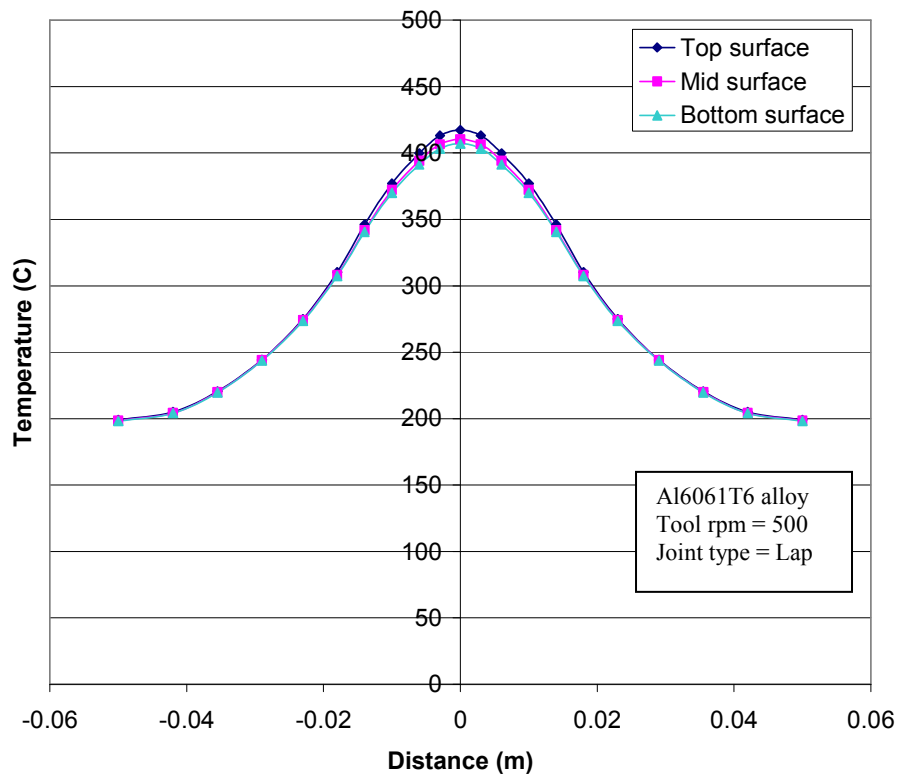


Figure 4.5.2. Instantaneous temperature profiles perpendicular to weld line at 140 mm/min.

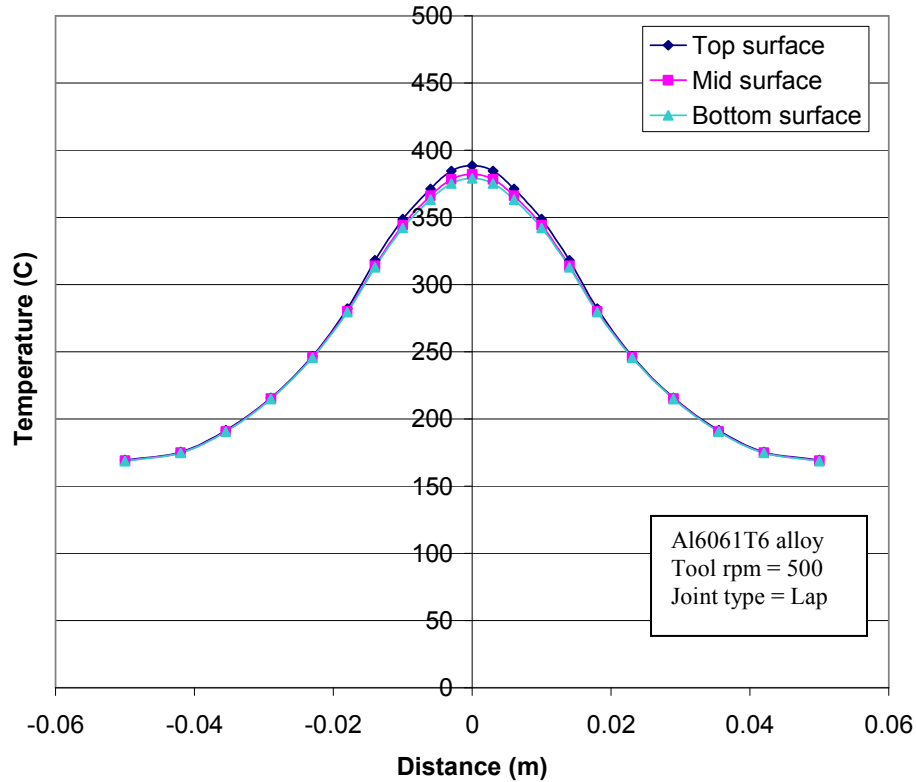


Figure 4.5.3. Instantaneous temperature profiles perpendicular to weld line at 180 mm/min.

Similar to the previous case, it is seen from the temperature history plots for Al6061-T6 alloy that the maximum or peak temperature obtained varied in between 460°C and 390°C for travel rates varying from 100 mm/min to 180 mm/min at constant tool rpm of 500 rpm. Also the minimum temperature obtained varied in between 247°C to 169°C. Good weld quality could be obtained for peak temperatures in between 410°C to 520°C which is possible with welding speeds in the range of 100 mm/min to 160 mm/min for a tool rpm of 500 rpm. For all the linear speeds a constant difference in temperature between top surface to mid surface and mid surface to bottom surface was seen. Similar to the earlier case it could be due to high thermal conductivity of material compared to the heat accumulation from thermal capacitance. This difference was 8°C in between the top surface and mid surface while 4°C was the difference between the mid surface and bottom surface temperature.

4.2.3 Case 3: Al7050-T7451 alloy

Figures 4.6.1, 4.6.2, and 4.6.3 show the instantaneous temperature profiles for tool travel rates of 100 mm/min, 125 mm/min, and 150 mm/min respectively at a distance of 190 mm from the start location of tool on Al7050-T7451 sheet. Tool travel rates were chosen through a literature review of various researchers [3, 13, and 14] such that the peak temperatures obtained were below the solidus temperatures of the alloy as required for a FSW process. The temperatures were recorded after a process time of 115 seconds, 92 seconds, and 76.5 seconds for linear speeds of 100 mm/min, 125 mm/min, and 150 mm/min respectively. Similar to previous cases, from the reference frame of heat source, the temperature distribution at these instants from a quasi-steady state heat transfer mode.

The computation time for linear speeds of 100 mm/min, 125 mm/min, and 150 mm/min was 132 seconds, 106 seconds, and 88 seconds respectively.

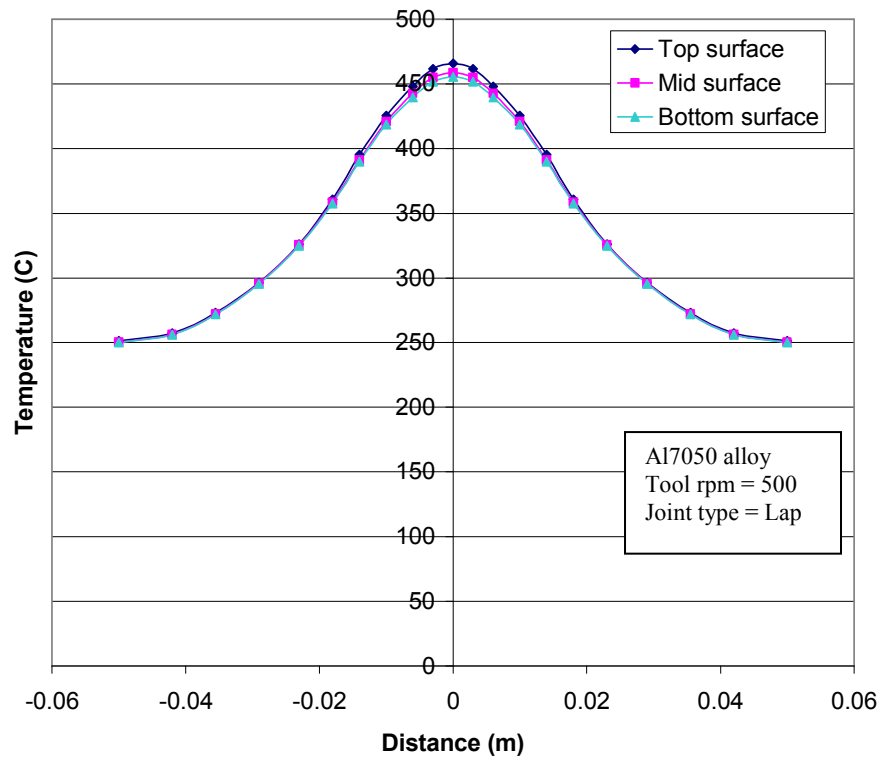


Figure 4.6.1. Instantaneous temperature profiles perpendicular to weld line at 100 mm/min.

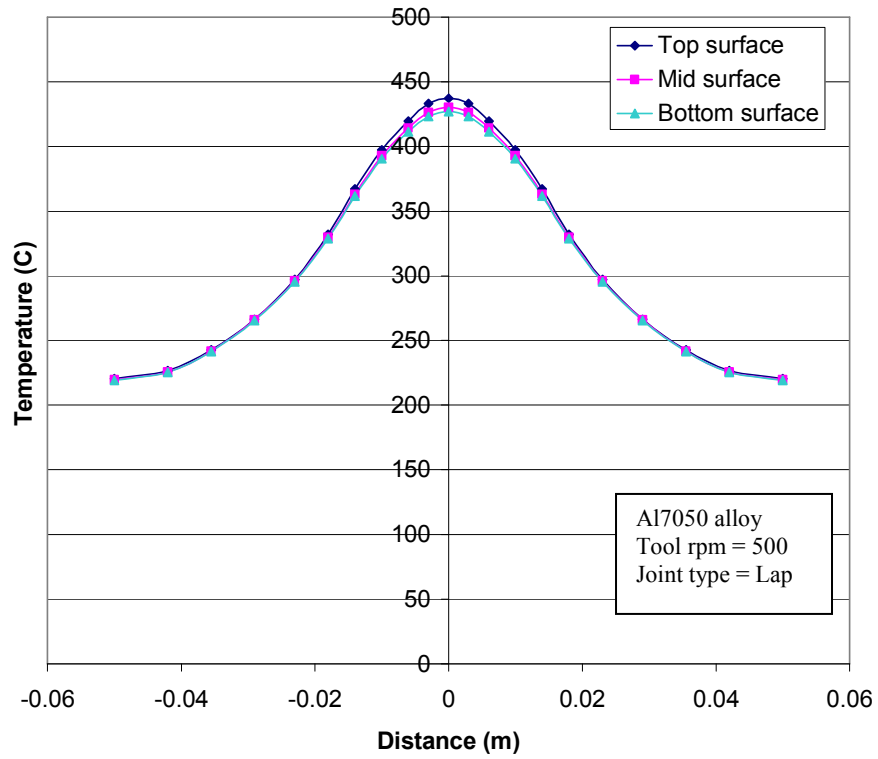


Figure 4.6.2. Instantaneous temperature profiles perpendicular to weld line at 125 mm/min.

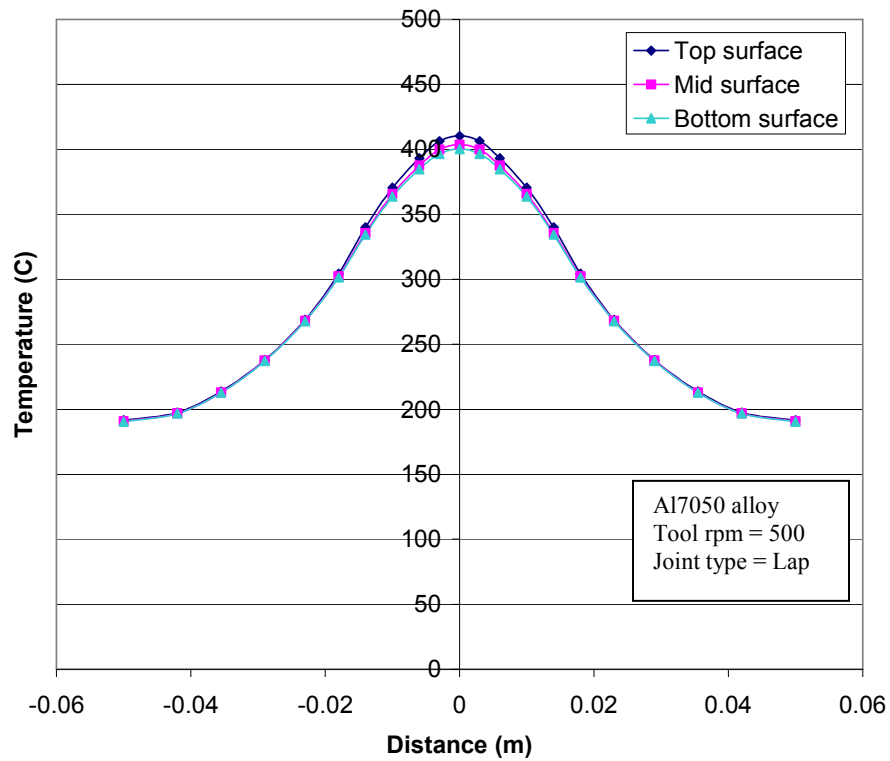


Figure 4.6.3. Instantaneous temperature profiles perpendicular to weld line at 150 mm/min.

It is seen from the temperature history plots for Al7050-T7451 alloy that peak temperatures obtained varied in between 465°C and 410°C for tool travel rates varying from 100 mm/min to 150 mm/min at constant tool rpm of 500 rpm. Good weld quality could be obtained for peak temperatures in between 410°C to 490°C which is possible with welding speeds in the range of 100 mm/min to 150 mm/min. For all the linear speeds a constant difference in temperature between top surface to mid surface and mid surface to bottom surface was seen. As in previous cases, it is due to high thermal conductivity of the workpiece compared to heat accumulation from thermal capacitance. Difference was 8°C in between the top surface and mid surface while 4°C was the difference between the mid surface and bottom surface temperature.

4.2.4 Case 4: Effect of Varying Tool Rotational Speeds on Workpiece Temperatures

The purpose of this case was to study the effect of rotational tool speed on peak temperatures. In this case for Al2024-T3 alloy the rotational speed of tool was varied from 400 rpm to 600 rpm for individual velocities of 140 mm/min to 220 mm/min. The rotational speed range is typical for FSW process. Table 4.1 shows the tabulated results for various rotational speeds applied. In FSW the joined material must be below solidus temperature, in this case 410°C. To identify the tool speed and rpm an additional study was performed in this case wherein the peak process temperature of around 410°C for Al2024-T3 alloy was kept constant and the tool travel rate and tool rotational velocity is varied in order to achieve the required temperature. The rotational speed was varied in between 400 rpm and 800 rpm while the tool travel rate was varied between 100 mm/min to 420 mm/min. Figure 4.7 shows the comparison between the tool travel rate and the tool rotational speed for a peak temperature of 410°C. It is seen from Figure 4.7 that for given increase in the tool rotational speed there has to be a proportional increase in the tool linear speed to achieve the required peak temperature. This is

probably due to amount of dwell time of tool needed to generate necessary amount of heat. The faster the linear speed for a given tool rpm less is the time to heat the workpiece.

Table 4.4

Summary of results for case 4 of lap weld

Tool linear speed (mm/min)	Rotational tool velocity (rpm)	Top surface peak temperature (°C)	Mid surface peak temperature(°C)	Bottom surface peak temperature(°C)
140	400	356	349	345
	500	438	430	426
	600	517	507	502
180	400	330	324	321
	500	406	399	395
	600	479	470	466
220	400	305	300	297
	500	375	368	365
	600	442	434	430

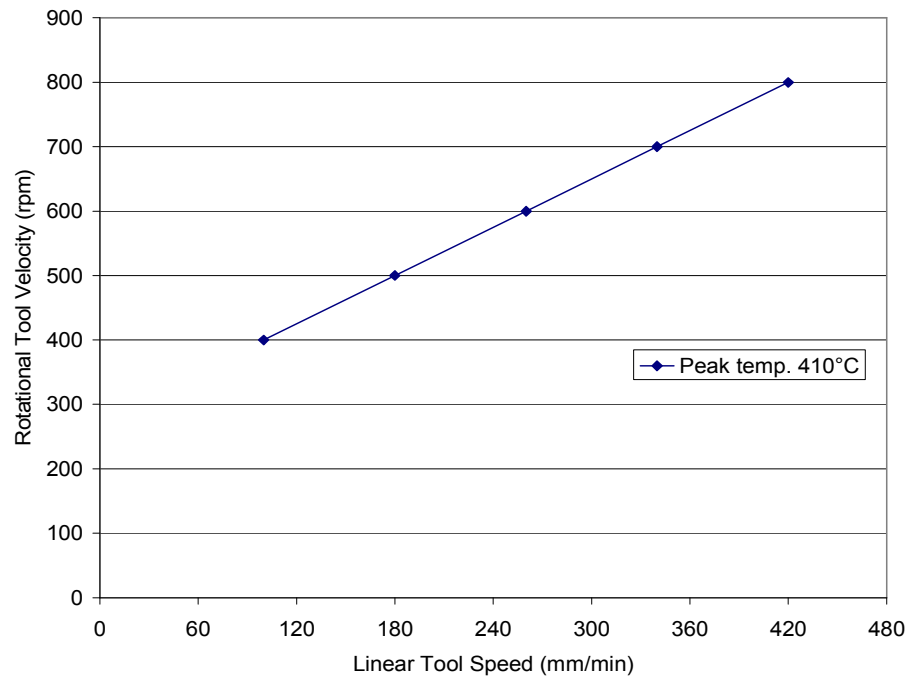


Figure 4.7. Comparison between rotational tool velocity and travel rate for Al2024-T3.

Summary of Results for FSW of Lap Weld

Table 4.5, 4.6, and 4.7 shows the summary of peak temperatures obtained for case 1, case 2, and case 3 respectively of lap weld.

Table 4.5

Summary of peak temperatures obtained for case 1 of lap weld

Material	Tool rotational velocity (rpm)	Tool travel rate (mm/min)	Top surface peak temperature (°C)	Mid surface peak temperature (°C)	Bottom surface peak temperature (°C)
Al2024-T3	500	140	438	430	426
		180	406	399	395
		220	375	368	365

Table 4.6

Summary of peak temperatures obtained for case 2 of lap weld

Material	Tool rotational velocity (rpm)	Tool travel rate (mm/min)	Top surface peak temperature (°C)	Mid surface peak temperature (°C)	Bottom surface peak temperature (°C)
Al6061-T6	500	100	463	456	453
		140	417	410	407
		180	389	382	379

Table 4.7

Summary of peak temperatures obtained for case 3 of lap weld

Material	Tool rotational velocity (rpm)	Tool travel rate (mm/min)	Top surface peak temperature (°C)	Mid surface peak temperature (°C)	Bottom surface peak temperature (°C)
Al7050-T7451	500	100	466	459	455
		125	437	430	427
		150	410	403	400

CHAPTER 5

CONCLUSIONS AND RECOMMENDATIONS

5.1 Conclusions

The original goal of this study was to develop thermal models of butt and lap weld which could be used to characterize the process and develop process specifications. For determining the temperature history during the FSW process, three dimensional models for FSW of butt and lap joints based on friction model were developed for specific experimental cases. The models were developed using LS-DYNA. The simulated outputs were in good agreement with the experimental results. Limitations of the models were that they were fit to match unknown variables like workpiece to backplate conduction and interplate thermal contact conductance to specific test data. Future work could involve determining these values experimentally. Parametric study was performed to investigate the effect of material, tool travel rates, and rotational speeds on temperature history. Based on the modeling effort and parametric study, the following conclusions could be drawn.

- A use of stepped contact conductance between lap joint sheets gave better correlation of simulated temperature data to experimental data. The thermal contact conductance used between the sheets was stepped from 2×10^6 W/m²C for the region immediately under the tool shoulder area to a level one-tenth as much. This simulated decrease in contact pressure between sheets beyond the tool shoulder region. Lower contact conductance at contact surfaces representing lower contact pressure will result in higher temperatures and asymmetric temperature fields.
- Use on equivalent convective coefficient into account for workpiece to backplate conduction allowed adequate correlation of test data to numerical data. A convective

coefficient of $300 \text{ W/m}^2 \text{ }^\circ\text{C}$ at the bottom surface of the sheet was assumed for a butt weld to account for the conduction between the sheets and the backup plate. In case of lapweld a high convective coefficient of $150 \text{ W/m}^2 \text{ }^\circ\text{C}$ was assumed at the bottom surface of the bottom sheet. These assumptions were consistent with other researcher's model methodology [3, 8, and 13] and yielded good comparison between simulated and experimental data. However additional testing to define the thermal pathways and thermal conductance would allow use of models for more general applications.

- The model dynamic friction coefficient of 0.3 for the butt weld and 0.15 for the lap weld permitted correlation of LS-DYNA temperature history plots to experimental data. These values were in conformity with a large number of published research data.
- For FSW lap welds, use of aluminium alloys with difference in thermal conductivity will probably require different process specifications (tool travel rate and rotational tool speed) to maintain optimum weld temperature.
- The effect of tool travel rate has been investigated for various alloy materials for both butt and lap welds. Lower the tool travel rate higher was the peak temperature obtained.
- By varying the tool travel rate or rotational tool speed, a constant difference in temperature between top surface to mid surface and mid surface to bottom surface was seen for both butt and lap welds. This ΔT for lap weld was lower compared to butt weld due to difference in processed zone. In lap weld the processed zone is through the complete thickness of two sheets leading to lower ΔT that's required for a good lap weld.
- The effect of rotational tool speed has been investigated for lap welds. For given increase in the tool rotational speed a proportional increase in the tool linear speed was necessary to achieve the required peak temperature.

5.2 Recommendations

- Additional lap weld FSW experiments need to be performed so that future better models could be developed and verified.
- More comprehensive heat generation model for lap welds is needed which uses a more realistic friction model and includes effects of plastic deformation.
- More accurate techniques or models for predicting the contact resistance in between the welded sheets need to be developed so that these could be accurately accounted for during the process model development.
- New clamping techniques need to be developed and characterized for reduction and possible eradication of any contact resistance present between the sheets to be lap welded.
- One of the possible techniques for reducing the heat loss through contact resistance during a FSW lap weld would be to use specialized thermal coatings on the faying surfaces that would enhance the overall heat transfer in between them.
- The concept of TCC should be studied in depth in order to systematically apply it to the lap weld process model. Few researchers have developed an approximation for the TCC with the exception being the relation between the heat transfer coefficient and the dimensionless pressure distribution at the faying surface developed by Xu et al. [21].

REFERENCES

LIST OF REFERENCES

- [1] Chao, Y. J. and Qi, W., 2003, "Heat Transfer in Friction Stir Welding-Experimental and Numerical Studies," ASME Journal of Manufacturing Science and Engineering, 125, pp. 138-145.
- [2] TWI, http://www.twi.co.uk/j32k/unprotected/band_1/fswintro.html
- [3] Khandkar, Mir Zahedul H and Khan, Jamil A., 2001, "Thermal Modeling of Overlap Friction Stir Welding for Al-Alloys", Journal of Materials Processing & Manufacturing Science.
- [4] Awang, Muccino, Feng, and David, 2005, "Thermo-Mechanical Modeling of Friction Stir Spot Welding (FSSW) Process: Use of an Explicit Adaptive Meshing Scheme", SAE International.
- [5] Gould, Jerry E. and Feng, Zhili, 1998, "Heat Flow Model for Friction Stir Welding of Aluminum Alloys", Journal of Materials Processing & Manufacturing Science, p 185-194.
- [6] Heurtier, P.; Desrayaud, C.; Montheillet, F., 2002, "A Thermomechanical Analysis of the Friction Stir Welding Process", Materials Science Forum, p 1537-1542.
- [7] Tang, W.; Guo, X.; McClure, J.C.; Murr, L.E.; Nunes, A., 1998, "Heat Input and Temperature Distribution in Friction Stir Welding", Journal of Materials Processing & Manufacturing Science, p 163-172.
- [8] Chao, Yuh J.; Qi, Xinhai, 1998, "Thermal and Thermo-mechanical Modeling of Friction Stir Welding of Aluminum Alloy 6061-T6", Journal of Materials Processing & Manufacturing Science, p 215-233.
- [9] Colegrove, P.; M. Painter; D. Graham, and T. Miller, 2000, "3 Dimensional Flow and Thermal Modeling of Friction Stir Welding Process, 2nd International Symposium on Friction Stir Welding, Sweden.
- [10] Zhu, X.K.; Chao, Y.J., 2002, "Effects of Temperature-Dependent Material Properties on Welding Simulation", Computers & Structures, p 967-976.
- [11] Song, Mingde; Kovacevic, Radovan; Ouyang, Jiahu; Valant, Mike, 2002, "A Detailed Three-Dimensional Transient Heat Transfer Model for Friction Stir Welding", 6th International Trends in Welding Research Conference, p 212-217.
- [12] Raikoty, Harsha; Ahmed, Ikram; Talia, George E, 2005, "High Speed Friction Stir Welding: A Computational and Experimental Study", Proceedings of the ASME Summer Heat Transfer Conference 2005, p 431-436.

- [13] Khandkar, Mir Zahedul H.; Khan, Jamil A.; Reynolds, Anthony P., 2002, "Input Torque Based Thermal Model of Friction Stir Welding of Al-6061", Trends in welding research : proceedings of the 6th International Conference, Callaway Gardens Resort, Phoenix, Arizona, p 218-223.
- [14] Khandkar, Mir Zahedul H, 2005, "Thermo-mechanical Modeling of Friction Stir Welding", PhD Dissertation, University of South Carolina.
- [15] MSC Software, <http://www.mscsoftware.com/products/patran.cfm>
- [16] LSTC, <http://www.lstc.com>
- [17] Goldak, J., 1984, "A New Finite Element Model for Welding Heat Sources", Metallurgical Transactions, Volume 15B, June, 1984, pages 299-305.
- [18] Ulysse, Patrick, 2002, "Three-dimensional Modeling of the Friction Stir Welding Process", International Journal of Machine Tools & Manufacture, p 1549-1557.
- [19] Russell, M.J.; Shercliff, H.R.; Threadgill, P.L, 2001, "Development and Application of an Analytical Process Model for Friction Stir Welding", p 225-234.
- [20] Frigaard, O; Grong, O; Bjornekleit, B; Midling, O.T, 1999, "Modeling of the Thermal and the Microstructure Fields during Friction Stir Welding of Aluminium Alloys", 1st International Symposium on FSW, June 1999.
- [21] Xu, L.; Khan, J.A, 1999, "Nugget Growth Model for Aluminum Alloys during Resistance Spot Welding", Welding Journal, p 367-s-372-s.
- [22] Raikoty, Harsha, 2005, "Thermal and Thermo-mechanical Aanalysis of High-speed Friction Stir Welding / by Harsha Raikoty", Wichita State University.
- [23] LS-DYNA Keyword Manual, www.lstc.com
- [24] ASM Handbook, <http://products.asminternational.org/hbk/index.jsp>
- [25] Madhusudana, C; "Thermal Contact Conductance", Mechanical Engineering Series.

APPENDIX

APPENDIX

LS-DYNA Keywords Used in Analyses

Few of the main cards used to define the model were as follows:

- ***CONTROL_IMPLICIT_GENERAL**
1, 0.5,
This card is used to define the analysis as an implicit analysis with 0.5 as the implicit timestep.
- ***CONTROL_SOLUTION**
2
This card is used to define the analysis as a thermal only analysis.
- ***CONTROL_THERMAL_TIMESTEP**
0,1.00,0.5,0.,0.,0.,0.
This card is used to define the timestep parameters for the thermal only analysis.
- ***BOUNDARY_THERMAL_WELD**
This card is used to define the thermal weld properties including the total heat to be applied and the area it has to be applied to.
- ***MAT_THERMAL_ISOTROPIC_TD**
This card is used to define the temperature dependent material properties for the model and it a maximum of 8 temperatures can be defined in this card.
- ***INITIAL_TEMPERATURE_SET**
This card is used to specify the initial process temperature of the model. It can be applied to a group of nodes or to all nodes in model.
- ***BOUNDARY_CONVECTION_SET**
This card is used to specify the convection coefficients to a group of element segments.
- ***CONTACT_AUTOMATIC_SURFACE_TO_SURFACE_THERMAL**
This card was used mainly for lap weld model. In this card the thermal contact conductance for a group of nodes can be specified.

LS-DYNA Keyword for Butt Weld

```
*KEYWORD
*TITLE
Case:Lap weld:Al2024-T3,140mmppm
*CONTROL_BULK_VISCOSITY
1.5 0.06
*CONTROL_CONTACT
```

```

0.1    0    2    0    1    1    1
0    0    10    0    4
*CONTROL_COUPLING
1    1    1    0                                1
*CONTROL_CPU
0
*CONTROL_DYNAMIC_RELAXATION
250  0.001  0.995  1e+30  0.9                0.04    0
*CONTROL_ENERGY
1    2    1    1
*CONTROL_HOURLASS
1    0.1
*CONTROL_OUTPUT
0    3    0    0    0                0
*CONTROL_SHELL
20    2    -1    0    2    2    1
*CONTROL_TERMINATION
95    0    0    0    0
*CONTROL_TIMESTEP
0.5  0.9    0    0    0    0    0    0
*DAMPING_GLOBAL
0    0
*DATABASE_BINARY_D3PLOT
0.5
$*DATABASE_TPRINT
$2
$=====
*CONTROL_IMPLICIT_GENERAL
1,0.5,
*CONTROL_SOLUTION
2
*CONTROL_THERMAL_SOLVER
$1,0,1,0.,0
1,0,3.,8,
*CONTROL_THERMAL_TIMESTEP
0,1.00,0.5,0.,0.,0.,0.
$=====
*NODE
1      0.3      0.0032      0.05
2      0.3      0.0032      0.0424224
3      0.3      0.0032      0.0355783
*
*
*
*
*
*
*
$=====
*MAT_THERMAL_ISOTROPIC_TD
1,2700,0,0.
-17.8,37.8,148.9,204.4,260,371.1,426.7,580
904,945,1004,1028,1052,1104,1133,1230
162,162,184,192,201,217,223,253
$=====
*BOUNDARY_SPC_SET

```

```

      7      0      1      1      1      1      1      1
*SET_NODE_LIST_GENERATE
7
20000,46354
*BOUNDARY_SPC_SET
      8      0      1      1      1      1      1      1
*SET_NODE_LIST_GENERATE
8
65000,91354
$=====
*SET_PART_LIST
1
1,2
*BOUNDARY_THERMAL_WELD
$
$
*DEFINE_CURVE
2
0,0
1,0
2,0
3,0
4,0
10,0
11,2500
15,2500
25,2500
146,2500
$300,1050
$=====
*BOUNDARY_PRESCRIBED_MOTION_RIGID
3,1,0,1,1
*DEFINE_CURVE
1,0,0.,0.,0.,0.,0
0.,0.0015
146,0.0015
$120,0.0015
$=====
*INITIAL_TEMPERATURE_SET
0,22
*END

```

LS-DYNA Keyword for Lap Weld

```

*KEYWORD
*TITLE
Case:Lap weld:Al2024-T3,140mmpm
*CONTROL_BULK_VISCOSITY
      1.5      0.06
*CONTROL_CONTACT
      0.1      0      2      0      1      1      1
      0      0      10      0      4
*CONTROL_COUPLING
      1      1      1      0

```

```

*CONTROL_CPU
0
*CONTROL_DYNAMIC_RELAXATION
250 0.001 0.995 1e+30 0.9 0.04 0
*CONTROL_ENERGY
1 2 1 1
*CONTROL_HOURLASS
1 0.1
*CONTROL_OUTPUT
0 3 0 0 0 0
*CONTROL_SHELL
20 2 -1 0 2 2 1
*CONTROL_TERMINATION
95 0 0 0 0
*CONTROL_TIMESTEP
0.5 0.9 0 0 0 0 0
*DAMPING_GLOBAL
0 0
*DATABASE_BINARY_D3PLOT
0.5
$*DATABASE_TPRINT
$2
$=====
*CONTROL_IMPLICIT_GENERAL
1,0.5,
*CONTROL_SOLUTION
2
*CONTROL_THERMAL_SOLVER
$1,0,1,0,0
1,0,3,,8,
*CONTROL_THERMAL_TIMESTEP
0,1.00,0.5,0.,0.,0.,0.
$=====
*NODE
1 0.3 0.0032 0.05
2 0.3 0.0032 0.0424224
3 0.3 0.0032 0.0355783
*
*
*
*
$=====
*MAT_THERMAL_ISOTROPIC_TD
1,2780,0,0.
20,100,200,300,400,500,545
850,900,950,970,1000,1080,1100
176,185,193,193,190,189,189
$=====
*SET_PART_LIST
1
1,2
*BOUNDARY_THERMAL_WELD
$
*DEFINE_CURVE
2
0,0

```

```

10,0
11,980
25,980
95,980
$=====
*BOUNDARY_PRESCRIBED_MOTION_RIGID
3,1,0,1,1
*DEFINE_CURVE
1,0,0.,0.,0.,0.,0
0.,0.00233
95,0.00233
$=====
*CONTACT_AUTOMATIC_SURFACE_TO_SURFACE_THERMAL
      7      3      0      0      0      0

1,1
,,2e6,0.001,0.001,
$=====
*CONTACT_AUTOMATIC_SURFACE_TO_SURFACE_THERMAL
      8      4      0      0      0      0

1,1
,,2e5,0.001,0.001,
$=====
*CONTACT_AUTOMATIC_SURFACE_TO_SURFACE_THERMAL
      9      5      0      0      0      0

1,1
,,2e4,0.001,0.001,
$=====
*INITIAL_TEMPERATURE_SET
0,25
*END

```